

Noncontact Multiphysics Probe for Spatiotemporal Resolved Single-Cell Manipulation and Analyses

Ayoola T. Brimmo, Anoop Menachery, Pavithra Sukumar, and Mohammad A. Qasaimeh*


Heterogeneity and spatial arrangement of individual cells within tissues are critical to the identity of the host multicellular organism. While current single-cell techniques are capable of resolving heterogeneity, they mostly rely on extracting target cells from their physiological environment and hence lose the spatiotemporal resolution required for understanding cellular networks. Here, a multifunctional noncontact scanning probe that can precisely perform multiple manipulation procedures on living single-cells, while within their physiological tissue environment, is demonstrated. The noncontact multiphysics probe (NMP) consists of fluidic apertures and “hump” shaped electrodes that simultaneously confine reagents and electric signals with a single-cell resolution. The NMP’s unique electropermealization-based approach in transferring macromolecules through the cell membrane is presented. The technology’s adjustable spatial ability is demonstrated by transfecting adjacent single-cells with different DNA plasmid vectors. The NMP technology also opens the door for controllable cytoplasm extraction from living single-cells. This powerful application is demonstrated by executing multiple time point biopsies on adherent cells without affecting the integrity of the extracted macromolecules or the viability of cells. Furthermore, the NMP’s function as an electro-thermal based microfluidic whole-cell tweezer is reported. This work offers a multifunctional tool with unprecedented probing features for spatiotemporal single-cell analysis within tissue samples.

1. Introduction

Heterogeneities in seemingly uniform cells within a tissue sample is now an established concept in cell biology.^[1,2] The

Dr. A. T. Brimmo, Dr. A. Menachery, P. Sukumar, Prof. M. A. Qasaimeh
Division of Engineering
New York University Abu Dhabi (NYUAD)
P.O. Box 129188, Abu Dhabi, UAE
E-mail: mohammad.qasaimeh@nyu.edu

Dr. A. T. Brimmo, Prof. M. A. Qasaimeh
Department of Mechanical and Aerospace Engineering
New York University
Brooklyn, NY 11201, USA

 The ORCID identification number(s) for the author(s) of this article can be found under <https://doi.org/10.1002/smll.202100801>.

© 2021 The Authors. Small published by Wiley-VCH GmbH. This is an open access article under the terms of the Creative Commons Attribution-NonCommercial-NoDerivs License, which permits use and distribution in any medium, provided the original work is properly cited, the use is non-commercial and no modifications or adaptations are made.

DOI: 10.1002/smll.202100801

concept is increasingly being appreciated in the analysis of complex diseases like cancer since therapeutics developed to target one tumor cell phenotype is not necessarily effective against neighboring cells with a different phenotype.^[3] Based on this, individual cell “omics” analysis^[4] is now the benchmark for a true systems-level understanding of how multicellular organisms function. The first step in assessing single-cells is isolation, and the conventional methods for single-cell isolation are micromanipulation, laser capture microdissection, and fluorescence-activated cell sorting.^[5] In the last few decades, these methods have increasingly applied as microfluidic technologies as they offer integrable platforms for downstream manipulation operations.^[6] Advances in this field include the use of microfluidic droplets, micro/nanowell, valves, and dielectrophoresis.^[7] These adaptations have contributed to the uncovering of important cell biology insights like the principle of DNA regulatory variation,^[8] resistance-linked genetic expressions within melanomas,^[9] complete lineage hierarchies of the developing lung,^[10] distinct stem-like gene expression signature of early stage metastasis of cancer,^[11] and the function of

mobile genes in human microbiome.^[12] However, while cellular processes such as proliferation, differentiation and reprogramming are transient in nature, most of these methods rely on procedures that dissociate cells from the tissue samples and cannot retain the original cell organization for multiple time point analyses.^[13,14] Hence, a robust spatiotemporal “omics” profiling of important cellular processes still remains a challenge for majority of the available techniques.^[15,16]

The ability to analyze the dynamics of single-cells, while retaining spatial configurations, is also important for a better understanding of cancer.^[17] For example, continuous crosstalk between immune cells in the tumor microenvironment have been reported to actively promote oncogenesis.^[18] In order to gain fundamental understanding of these intratissue interactions, tools capable of multiple time-point sampling of living single-cells, while in their natural physiological environment, are paramount. A few methods have now been successfully developed to achieve this by physically inserting nanopipettes into the cell, and can broadly be classified as nanopipettes^[19,20] and Fluid Force Microscopy (FluidFM).^[21] Some groundbreaking applications of these technologies include a

combination of nanopipettes with dielectrophoresis to trap single DNA and protein molecules,^[22] and a demonstration of the ability of cells to withstand several picoliters of cytoplasm extraction with the FluidFM.^[23] Nevertheless, since both nanopipettes and FluidFM involve physical penetration of the cell, they typically result in cell lacerations of about 1–3% of the cell size, which could be detrimental to subsequent cell function. Furthermore, such invasive insertions could hinder the practicality of probing single cells repeatedly at different time points.

Here, we report a noncontact multiphysics probe (NMP) that can be precisely controlled to genetically manipulate and analyze living single-cells within tissue-like culture. The NMP is a multifunctional tool that combine the concepts of electropermealization (EP),^[24] hydrodynamic flow confinement (HFC)^[25] and contactless scanning probes to achieve noncontact spatiotemporal resolved single-cell manipulation (Figure 1), and utilizes advanced direct laser writing 3D printing^[26] as its main fabrication procedure to enable rapid prototyping. While other pioneering substrate^[27] and probe-based^[28] EP methods have previously demonstrated multiple time point sampling of live cells, the NMP sets apart with its noncontact function (minimally invasive) and adjustable spatial ability (multiplexed single cells) while maintaining spatiotemporal resolution. The NMP was developed by building on the microfluidic probe and multipoles concepts^[29–31] for hydrodynamically confining liquids on an open substrate. In the current work, we advanced these concepts to multiphysics constructs, by leveraging our previously developed techniques of 3D printing microfluidic probes to seamlessly integrate enabling structures.^[32,33] The otherwise manual vertical positioning of the probe—with respect to the cell—was also automated using image recognition models and validated structural mechanism correlations. These enabled precise simultaneous confinements of reagents and electric fields with a single-cell precision, in order to facilitate noncontact multiparametric manipulation operations while retaining cellular spatial configuration.

The multiphysics utility of the resulting NMP was analyzed by transferring varying size exogenous molecules into cells in adherent culture. This enabled a comprehensive characterization of the EP-based molecular transfer response of cells in the nonrounded adherent state. In addition, the spatial precision of the NMP's electro-fluidic fields was demonstrated by precisely patterning an adherent cell cluster with impermeable dyes, and its unique spatiotemporal genetic manipulation capabilities was demonstrated by transfecting multiple single-cells, within the same vicinity, with different DNA plasmid vectors. Remarkably, we also show that the NMP is applicable for performing controllable extraction of the cytoplasmic content of single-cells—either as a one-time point excisional biopsy or as multiple time points incisional biopsies—without affecting the integrity of the extracted RNA or cell viability. Interestingly, this powerful cell biopsy technique portrays potential for separate collection of subcellular compartments of a single-cell target. Furthermore, with a subtle alteration of the electrical configuration, the NMP can facilitate heat dependent enzymatic dissociation of whole single-cells for total expression assays.

2. Results

2.1. Noncontact Multiphysics Probe

The NMPs described herein were fabricated by 2-photon lithography based 3D printing^[26] and their surfaces were made electrically conductive by direct gold sputtering. The complete device consists of an assembly of a probe handle, probe to holder adapter, fluidic pins, and the NMP (Figure 1a; and Section S1, Supporting Information). The hump shaped electrode, which provides a concentrated electric field, was located on the tip of the NMP and the counter electrode consists of a transparent conductive indium tin oxide (ITO)-coated glass substrate. In the two-aperture (microfluidic dipole)^[29] and single hump (monoplex) electrode configuration adopted for single-cell targets, the size of the electrode was 25 μm base radius and height, whereas the fluid apertures were designed with radii of 15 and 30 μm for the inlet and outlet apertures, respectively. The dimensions of the electrode were selected to ensure a uniform electric field across the surface of the target cell (Section S2, Supporting Information). A 100 μm center-to-center spacing (*S*) between both apertures allowed for an electrode placement at that position. These dimensions define the fluidic confinement and electric field footprints (inset Figure 1a and top row of Figure 1b). To achieve multiplexed probing of single-cells, the electrodes and apertures were doubled to a four-aperture (microfluidic quadrupole)^[31] and two hump (duplex) electrode configuration (bottom row of Figure 1b).

During operation, the device works in a pin-plate electrode setup, with the hump representing the “pin” electrode and the ITO-coated substrate as the counter “plate” electrode. The hump electrode confines an electric field to the target cell (top inset Figure 1a), and a syringe pump driven push-pull flow configuration^[25] through the apertures create the HFC of the reagent around the cell (bottom inset Figure 1a). The electric field (*E*) between the hump and the substrate can be calculated based on the fundamental Maxwell relation

$$\oint E \cdot dA = \frac{Q}{\epsilon_0} \quad (1)$$

Where *E* is the electric field, *A* is the area enclosing the surfaces, *Q* is the net charge, and ϵ_0 is the permittivity of the immersion media. Calculation of the electric field is based on modeling a Gaussian surface around the electric charge distribution and evaluating the resulting electric flux. Using 3D finite element modeling, the electric field across the substrate is calculated and displays a sharp convergence to the target area due to; (1) the small area of the hump electrode relative to the bottom substrate, and (2) the electric field bending phenomena (Figure 1c; and Section S2, Supporting Information). Precise control of this convergent field permits isolated exposure of single-cells to electric fields above the threshold of EP.

For a given tip-substrate spacing (*G*), the shape and span of the HFC is dependent on the ratio between the outlet and inlet flow rates ($Q_{\text{out}}/Q_{\text{in}}$)^[30] while, the magnitude of the flow velocity is dependent on the flow rates at the inlet and outlet apertures (Figure 1d; and Section S3, Supporting Information). Using a point-source aperture approximation, exact solution of the microfluidic dipole's velocity profile is defined by^[29]

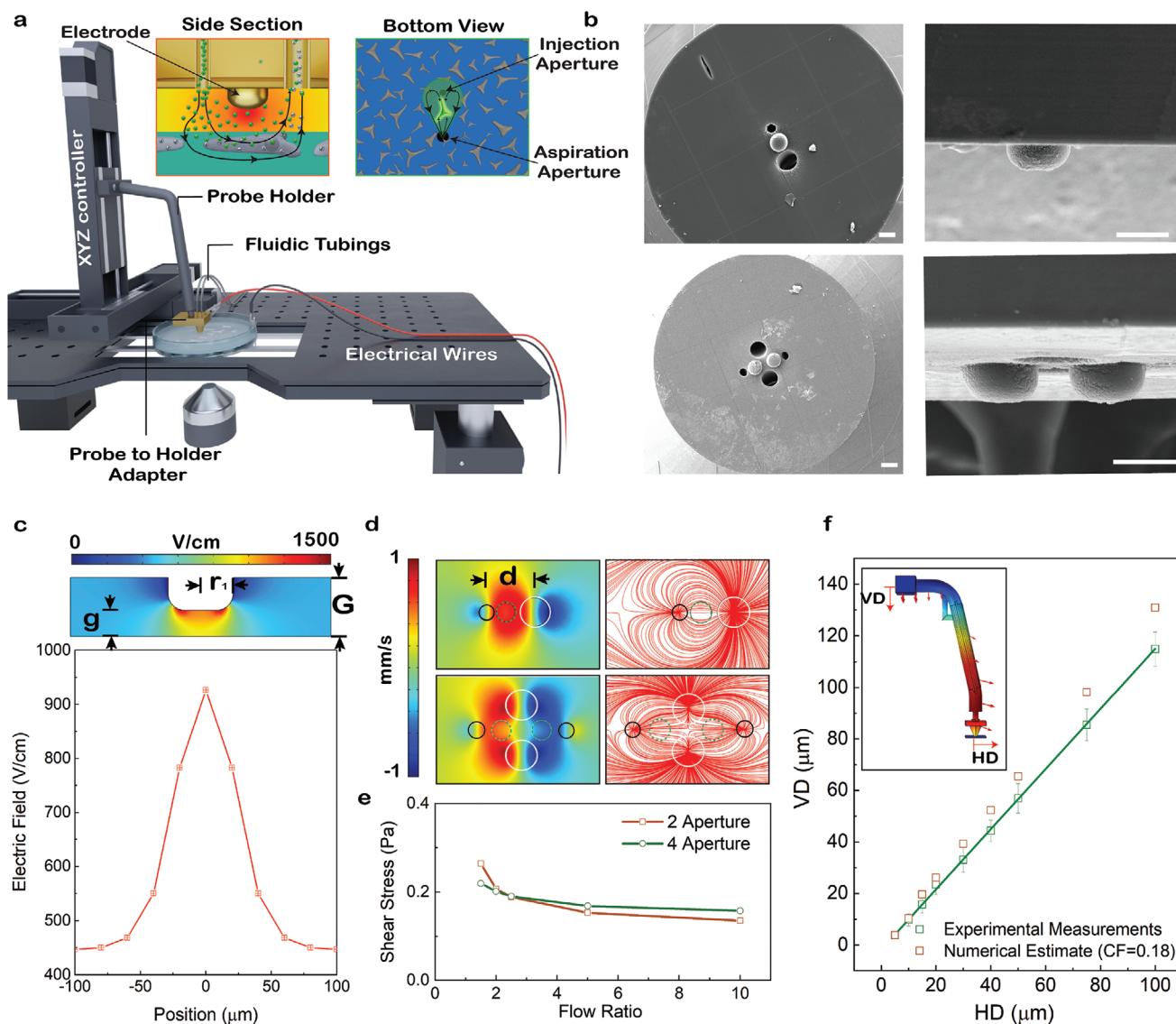


Figure 1. The noncontact multiphysics probe (NMP). a) 3D illustration of the NMP apparatus with sectional views showing the simultaneous confinement of an electric field (left inset) and reagents (right inset) to a single-cell target for nucleic acid transfer through the cytoplasm membrane. In this setup, reagents are passed through the tubings using a high precision syringe pump and the electrical signals are passed to the electrodes using a signal generator. b) Scanning electron microscopy micrographs with the top (left) and side (right) views of the two apertures/one electrode (top row) and four apertures/two electrodes (bottom row) NMPs. Scale bar is 50 μm . c) Finite element modelling based electric field contour (top) and magnitudes across the bottom substrate (bottom) shows confinement of the high electric field to areas directly beneath the hump electrode. A 2 V potential difference was applied with an electrode-substrate gap of 20 μm . d) Velocity profile (left) and streamline (right) of the two apertures (top row) and four apertures (bottom row) fluid flow confinement with an inlet aperture flow rate (Q_{in}) of 0.25 $\mu\text{L min}^{-1}$ and a flow ratio ($Q_{\text{out}}/Q_{\text{in}}$) of 2. All obtained from finite element modelling. e) Shear stress experienced by target cells beneath the electrodes as a function of flow ratio with a constant outlet aperture flow rate (Q_{out}) of 0.5 $\mu\text{L min}^{-1}$. f) Experimental correlations between the vertical displacement (VD) and horizontal displacement (HD) of the probe handle for the image recognition enabled tip-substrate gap manipulation. Error bars are standard deviation from 4 repeats. A finite element based model, with a glass-NMP coefficient of friction of 0.18, was used as validation.

$$(x, y) = \frac{Q_{\text{in}}}{2\pi G} \left[\left(\frac{x-d}{2} - \frac{\alpha(x-d)}{2} \right) \hat{x} + \left(\frac{1}{(x-d)^2 + y^2} - \frac{\alpha}{(x+d)^2 + y^2} \right) \hat{y} \right] \quad (2)$$

Where x and y are the positional coordinates outlining the HFC footprint under the Cartesian coordinates, d is the spacing between the apertures, G is the tip-substrate gap, and α is $Q_{\text{out}}/Q_{\text{in}}$. The characteristic length of the dipole footprint (L_D), is given by^[29,31]

$$L_D = d \left(\frac{\alpha + 1}{\alpha - 1} \right) \quad (3)$$

The velocity profile and characteristic length equations for other microfluidic multipole configurations have similar forms.^[30,31] An important consideration in microfluidic-based manipulation and analyses of cells is to ensure that imposed shear stress does not exceed physiological limits. Hence, calibration of the NMP parameters for low shear stress is important. According to Stokes law, the shear stress imposed by the HFC is proportional to the tangential flow velocity (\vec{v})

$$\tau(x, y) = \frac{6\eta}{G} \vec{v}(x, y) \quad (4)$$

Where η is the fluid's viscosity. Based on our selected aperture sizes and an electrode-substrate gap of 20 μm , we numerically calibrate for flow rates with imposed shear stresses well below the "critical shear stress levels" of mammalian cells (Figure 1e). According to Equation (4), shear stress values can be further reduced either by increasing the tip-substrate gap or reducing the flow rate (Section S3, Supporting Information).

From Equations (1), (2), and (4), it is evident that G is an important parameter that controls the NMP electrical and fluidic manipulation parameters. This parameter has historically been controlled using visual techniques that are prone to human error. In this work, automated control of G was achieved using an image recognition technique based on Kernelized Correlation Filters.^[34] The procedure depends on tracking and measuring the horizontal displacement (HD) resulting from a downward vertical displacement (VD) when the tip of the electrode is in contact with the bottom substrate. Since the onset of HD coincides with the zero VD, VD was correlated with HD for a given probe holder stiffness and electrode/glass slide coefficient of friction. The experimental correlation between VD and HD were also numerically validated with a friction coefficient of 0.18. Subsequently, zeroing of VD was achieved by tracking and measuring HD using the image recognition module (Figure 1f; and Video S1 and Codes S1, Supporting Information), and using the deduced correlation to calculate VD. Upon zeroing VD, the Z axis of the XYZ controller was automated to position the electrode's tip at the desired gap G . In order to facilitate this procedure, "zeroing areas" void of cells were reserved on the substrate and gentle lowering of the NMP was ensured to avoid abrasion of the electrode's tip.

2.2. Delivery of Extracellular Macromolecules into Cells

Creating temporary pores on cell membranes via the application of electric pulses provides the basis for transporting molecules in and out of biological cells via EP.^[35] This cell manipulation technique has been used extensively for the insertion of biomarkers, proteins, drugs, genes, and other macromolecules (e.g., Ca^{2+} ions) into cells.^[24] In general, experimental outcomes have been in agreement with the available theoretical framework. However, majority of these studies have been carried on suspended cells and preliminary indications suggest that modification of these theories will be required for applications on cells in adherent cultures.^[36] Hence, more comprehensive characterizations are required for better understanding of the EP-based transfer of molecules into adherent cells.

The suitability of the NMP as a characterization tool for the transfer of extracellular molecules into adherent cells via EP was first validated by delivering fluorescently labelled impermeable molecules of different sizes (0.68 kDa propidium Iodide and 250 kDa Fluorescein isothiocyanate-dextran into mammalian cells. This demonstration relies on intracellular excitation of propidium iodide (PI) and isothiocyanate-dextran (FITC-Dextran) fluorescence as an indicator of compromised cell membrane. In order to expand the target area from single-cells to a cluster of cells, the NMP configuration used for this characterization distributes multiple humps across the entire NMP's tip (Figure 2a; and Section S4, Supporting Information). The NMP's electrodes were positioned 20 μm above the target cells cultured on the counter electrode substrate and simultaneous activation of the HFC (PI dissolved in the EP buffer, $Q_{\text{out}} = 0.5 \mu\text{L min}^{-1}$, 30 s duration) and DC pulse parameters (2 V, 10 Hz, rectangular pulses, 100 μs pulse width, 1 s duration) resulted in transfer of PI into the target breast cancer cells MCF-7 (Michigan Cancer Foundation-7), as indicative of the cells labelled with red stains in Figure 2b. We also demonstrate the ability to reduce the target footprint by simply adjusting flow ratios ($Q_{\text{out}}/Q_{\text{in}}$) from 4 (Figure 2b (top row)) to 10 (Figure 2b (bottom row)). Restriction of the resulting PI stained cells to the HFC footprint confirms confinement of the PI solution from the surrounding fluid.

Given that EP pore sizes are dependent on pulse width,^[24] and diffusion of molecules through the cell membrane is time dependent, we selected pulse width and the HFC exposure time as characterization parameters for the dosing rate. Due to the complexity of biological membranes—which include uneven surface charge distribution, nonuniform membrane thickness, interference from intracellular cytoskeleton—accurate theoretical relationship between pore size and pulse-width are not feasible.^[24] Hence, we rely on experimental characterizations to obtain the relationship. As expected, these parameters regulated the EP induced pore size on four different adherent cell types as indicative of the increase in PI intensity with HFC exposure time and pulse width (Figure 2c,d). The percentage entry (number of fluorescence cells/number of target cells) of macromolecules is also expected to be dependent on the applied field strength and this relation was characterized with 250 kDa FITC dextran molecules (Figure 2e). As a control, in the absence of electric field, minimal change in fluorescence intensity was observed which confirms the dependence of molecule intake on EP (Figure 2c,e; and Section S5, Supporting Information). An interesting finding was that the time provided for cell attachment to the ITO coated glass slides significantly affected delivery of PI—24 h cell attachment resulted in significantly increased dye intake than 3 h cell attachment (Section S6, Supporting Information). This clearly highlights an increase in EP potential with increased cell stretching in adherent culture. While the exact dynamics is not fully understood, we attribute it to the reduction of folds and microvilli upon full adhesion/stretching which is expected to lead to an increase in permeability (see Section S6 for more details, Supporting Information). Furthermore, to demonstrate spatiotemporal control, we transfer PI molecules into an adherent culture of MCF-7 cells in a pattern that spelt "NYU" (Figure 2f; Video S2 and Section S7, Supporting Information). This

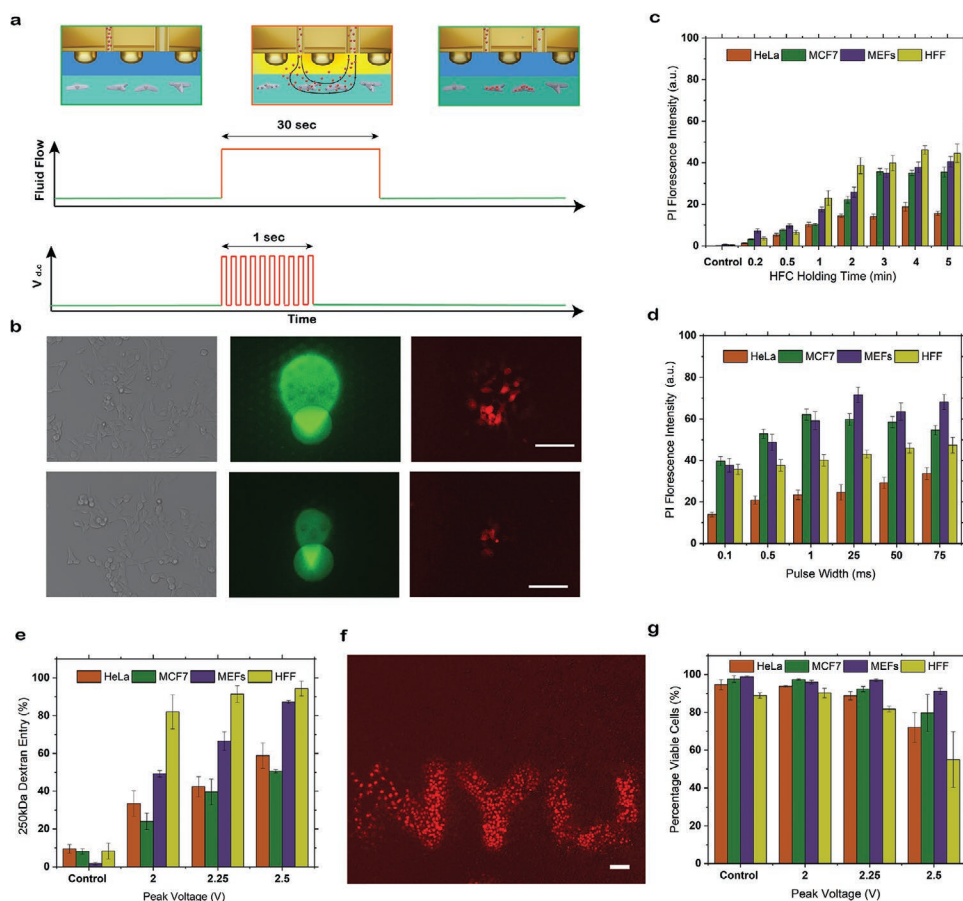


Figure 2. Electroporation (EP) of adherent cells and delivery of extracellular macromolecules. a) Step by step schematics (top) and time trace (bottom) of EP based dye transfer into cells. With a distribution of the hump electrode across the NMP's tip, all cells beneath the probe experience the electric field but only the cells exposed to the HFC receive the molecules. b) Bright field images (left), FITC fluorescence images during HFC activation (middle), and red fluorescence images after EP (right) of the target area within an MCF-7 culture. $Q_{out}/Q_{in} = 4$ (top row) and $Q_{out}/Q_{in} = 10$ (bottom row). Pulse width was 100 μ s and HFC exposure was 30 s. Scale bars are 50 μ m. c) PI fluorescence intensity of different target cell types after simultaneous EP (100 μ s) and exposure to PI reagent HFC with varying duration. d) PI fluorescence intensity of different target cell types after 3 min exposure to the PI reagent HFC and 1 s exposure to electric pulses of varying pulse width. e) Percentage entry of 250 kDa FITC dextran to different target cell types after 3 min exposure to the FITC dextran HFC and 1 s exposure to 10 Hz, 50 ms electric pulses of varying peak voltage. f) Red fluorescence image of the patterned MCF-7 cells after simultaneous exposure to the HFC of PI dissolved in EP buffer and 2 V/10 Hz electric pulses with 50 ms pulse width, while operating in the scanning mode. Scale bar is 100 μ m. g) Cell viability 24 h after exposure to HFC of plain EP buffer (3 min exposure time) as a function of peak voltage (50 ms pulse width). Percentage viability drops below 90% at 2.5 V hence, indicating the onset of the threshold value for the NMP while operating with a DC pulse. Error bars represent standard error from at least 40 cells and 4 repeats.

highlights the advantage of the NMP as a dynamic tool with unprecedented spatiotemporal control for EP-based cell manipulation applications.

Application of high electric fields could lead to irreversible EP and subsequently cell death. If the threshold electric field strength is exceeded, the number and size of generated pores surpasses the tolerable limit and hence results in membrane rupture.^[24] As such, cell viability is an important indicator used to measure the success of reversible EP and we validated the viability of our electrical parameters by performing a live/dead assay on the target areas 24 h after EP—3 min fluid exposure of plain EP buffer with no fluorescent dye, and 1 s exposure of DC rectangular pulses of 50 ms width (Figure 2g). These HFC and electric pulse parameters were selected based on observed saturation of PI intake at these values (Figure 2c,d).

2.3. Multiplexed Single-Cell Transfection

The approach of delivering genes as plasmid DNA vectors via EP is a potent alternative to the use of recombinant viruses.^[37] Having established the capability to deliver molecules of different sizes into the cytoplasm, we used the NMP to deliver mammalian expression vector for green fluorescent protein (pCMV-GFP) to target MCF-7 cells in their adherent culture. As expected, the target cell footprint bounded by the HFC precisely matched the transfected cell region, as indicated by the presence of green fluorescent MCF-7 cells, 24 h after EP (Section S8, Supporting Information). We also characterized transfection efficiency as the ratio of number of fluorescence cells to the number of target cells for MCF-7 and primary mouse cell (Mouse Embryonic Fibroblast (MEFs)). Transfection efficiencies between 2% and 20% were obtained for pCMV-GFP and

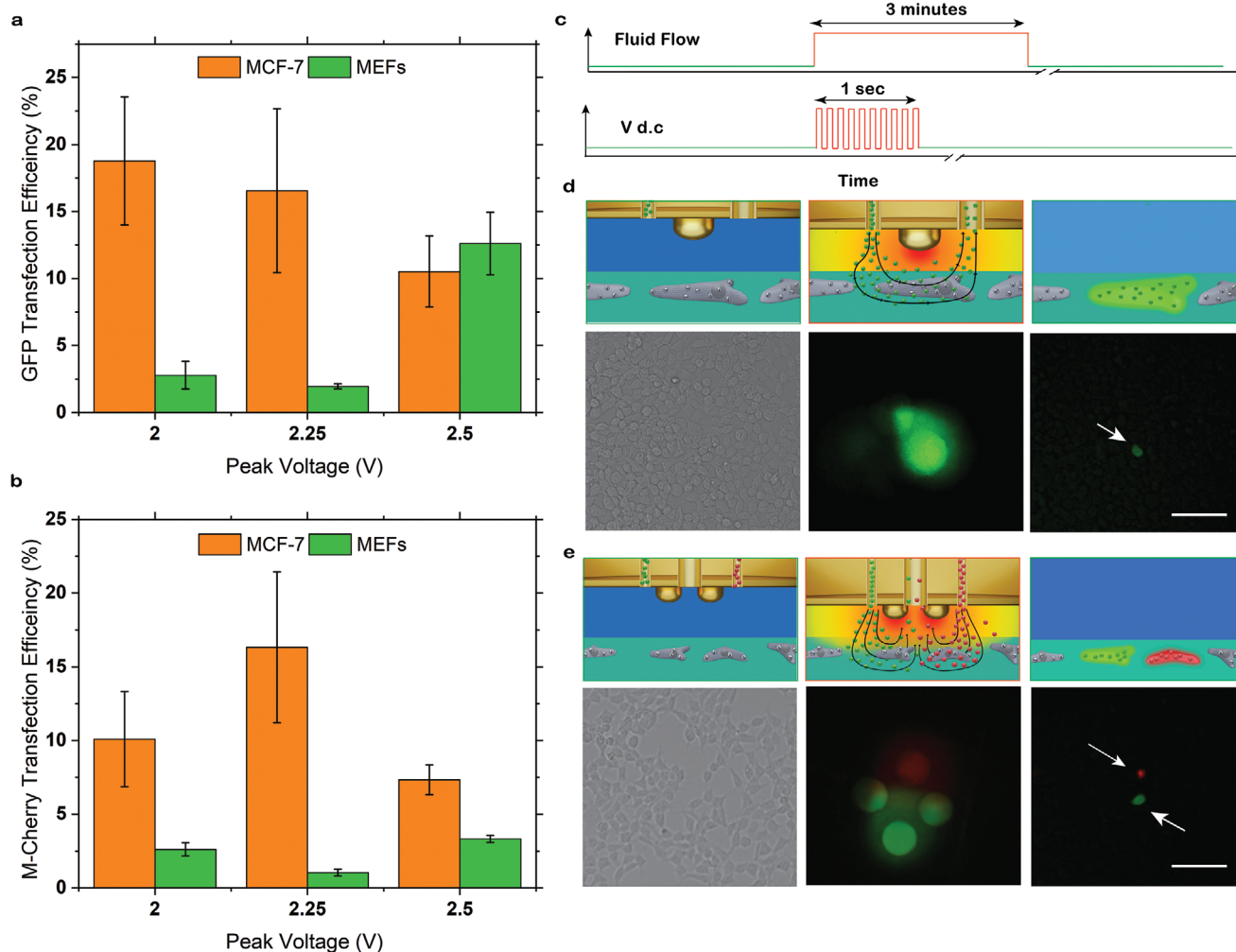


Figure 3. Multiplexed single-cell transfection. a) pCMV-GFP transfection efficiency in MCF-7 and primary Mouse Embryonic Fibroblast (MEFs) cells as a function of DC pulse amplitude. b) mCherry2-C1 transfection efficiency in MCF-7 and MEFs cells as a function of DC pulse amplitude. Electric pulse properties in a) and b) are 10 Hz frequency, 50 ms pulse width and 1 s duration, and the HFC is obtained at $Q_{out}/Q_{in} = 2$ and exposure time of 3 min. Error bar represents standard deviation from minimum of 4 separate experiments. c) Time trace of the HFC and DC electric pulses used for single-cell transfections. d) Step by step schematics of the single-cell transfection process (top row) and corresponding bright field (left bottom), fluorescence image during EP (middle bottom), and green fluorescence image 24 h after transfection with pCMV-GFP plasmid (right bottom). The HFC in the middle bottom panel is labeled with green fluorescein sodium salt to aid HFC visibility. Scale bar is 100 μm. e) Step by step schematics of the multiplexed single-cell transfection process (top row) and corresponding bright field (left bottom), fluorescence image during EP (middle bottom), and merged green and red fluorescence image 24 h after transfection with pCMV-GFP and mCherry2-C1 (right bottom). Scale bar is 100 μm. The HFCs in the middle bottom panel are labeled with green fluorescein sodium salt for visibility and the top half is modified with a red filter on ImageJ. DC electric pulse properties used in d) and e) are 10 Hz frequency, 50 ms pulse width and 1 s duration, and the HFC is obtained at $Q_{out}/Q_{in} = 4$ and exposure time of 3 min.

monomeric red fluorescent proteins (mCherry2-C1) upon varying the pulse amplitude up to 2.5 V (Figure 3a,b)—after which there is a decrease in viability as shown in Figure 2g. These efficiencies are in-line with those obtained in previous attempts in transfecting single-cells, while in adherent culture.^[38] Nevertheless, based on the characteristically unsymmetrical nature of the electric field generated by the substrate based electrode, we postulate that modification of the electrode's configuration and alternating of the electric field direction could increase the susceptible area for DNA transfer.^[39,40]

To validate the use of the NMP for single-cell targets, a monoplex electrode was used to concentrate the electric field to a smaller footprint. We show successful transfer of PI into

single-cell targets (Video S3, Supporting Information) and demonstrate the ability to perform single-cell transfection (time trace in Figure 3c) by simultaneous confinement of the pCMV-GFP reagent (3 min exposure time) and the DC rectangular electric pulse to a single-cell (top row Figure 3d). A representative Figure 3d shows a green fluorescence cell at the target area obtained 24 h after electroporation with the NMP, which confirmed successful single-cell transfection with pCMV-GFP plasmid. Achieving such with conventional substrate-based microfluidic devices could be associated with difficulties in culturing, and selectively targeting, cells within microscale channels^[41,42] hence, substrate based microfluidics are mostly applied for electroporation of cells in the suspended state.^[43]

On the other hand, microelectrodes have been demonstrated to electrically transfected single-cells while maintaining spatial resolutions in the adherent culture.^[28,38] However, since these devices do not involve fluid confinement, it is challenging to control and scale up for simultaneous delivery of different genes to neighboring multiple single-cells. In this work, we show that the NMP technology can be easily adaptable for simultaneous multiplexed single-cell gene delivery. This was achieved by implementing the duplex electrode and microfluidic quadrupole configuration (bottom row of Figure 1b) to simultaneously deliver two different plasmids to adjacent cells in the same vicinity (top row of Figure 3e). Visible green and red fluorescent single-cells confirmed isolated transfection of adjacent single-cells with the pCMV-GFP and mCherry2-C1 plasmids respectively (bottom row of Figure 3e). The NMP multiplexed transfection feature can be extended for an increased number of single-cells by inserting additional electrodes and

microfluidic multipole configurations.^[25,30,31] Such multiplex features remarkably open the door to programming single-cells with phenotypes variants for controlled studies on genomic diversity within tissue cultures.^[44]

2.4. Single-Cell Biopsies

The ability to extract cytoplasmic contents from single-cells without dissociating them from their physiological environment provide fundamental omic insights while retaining cellular and tissue integrity. The NMP enables noncontact cytoplasmic extraction (biopsy) from single-cells by using a confinement of hypoosmotic EP buffer ($Q_{out}/Q = 4$) to collect single-cell cytoplasm released thru EP (Figure 4a). While EP is commonly performed with DC pulses, when higher electric fields are used to increase pore sizes, there is a risk of inducing pH changes

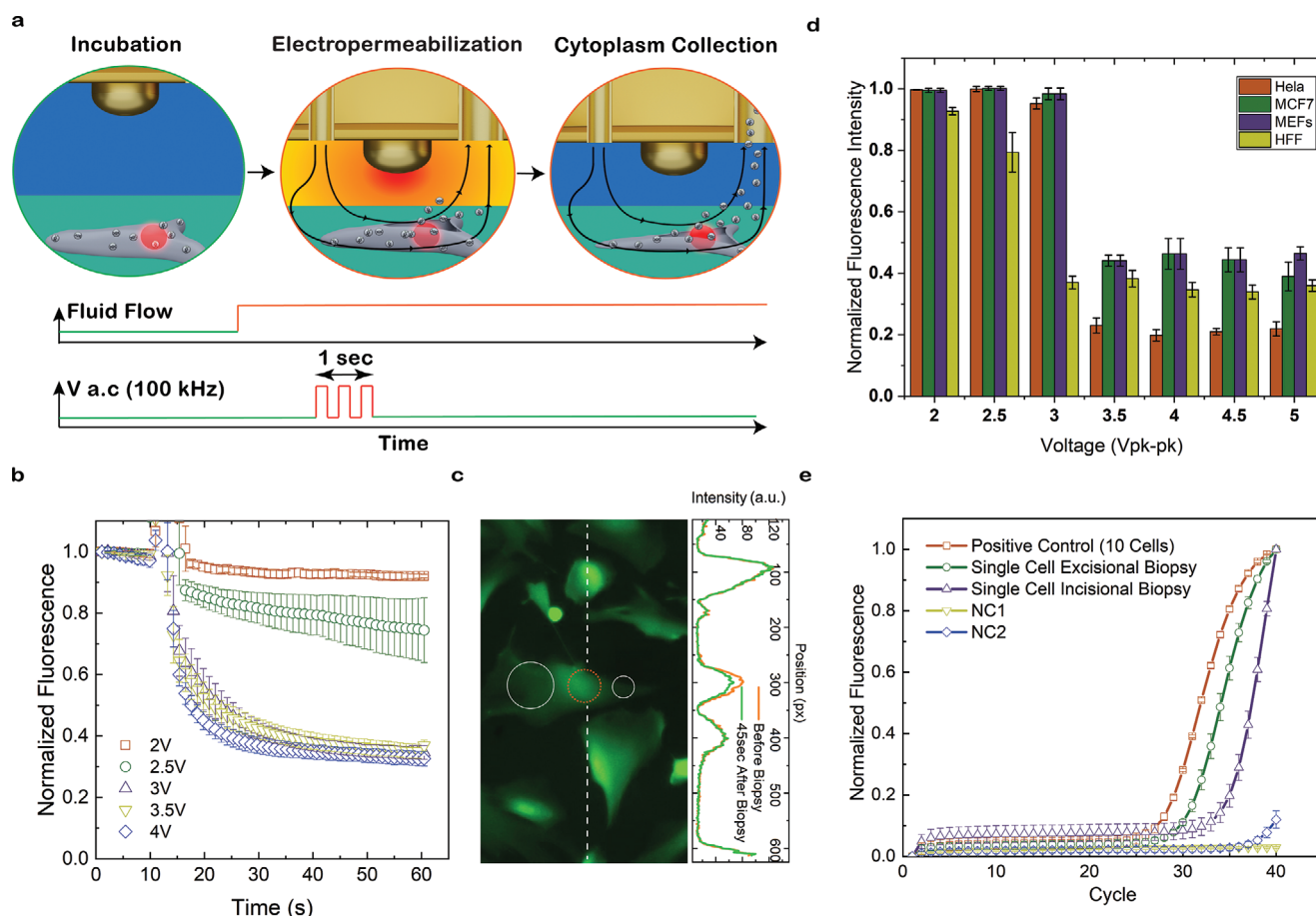


Figure 4. Controllable single-cell biopsies. a) Step by step schematics (top) and time trace (bottom) for the single-cell biopsy operation of the NMP. b) Normalized FITC fluorescence intensity of HFF before (0–15 s) and after (15–60 s) cell biopsies, as a function of applied pk–pk voltage (100 kHz, 1 s duration). Error bar indicates standard deviation from 4 individual measurements from different cells. c) Green Fluorescence image of calcein AM labeled HFF cells after incisional cell biopsies. Plot at the right side represent the spatial fluorescence intensity across the dotted line sections to quantify the green intensity drop in the target cell and show intensities of neighboring single-cells do not drop after targeted incisional biopsy. White dotted circles represent the positions of the inlet and outlet apertures, while the red dotted circle represents the position of the hump electrode. Diameter of the outlet aperture is 60 μm . d) Normalized FITC intensity of target HeLa, MEFs, MCF, and HFF cells 1 min after single-cell biopsies as a function of pk–pk voltage. Error bar indicates standard deviations from 4 individual measurements from the same single-cell sample. e) Mean qPCR amplification curve for RNase P RNAs for incisional and excisional HFF biopsies along with positive controls (10 cells preprocessed with chemical lysis), negative controls (NC 1 – NMP culture media sampling before biopsy and NC 2 – NMP sampling 5 min after biopsy). Error bars indicate standard deviation of 4 individual measurements collected from the same single-cell sample, i.e., the biopsy from a single-cell was divided into 4 qPCR samples.

due to electrolysis. As such, for the biopsy implementation, the NMP was operated with AC waveforms, where electrodes alternate as anode and cathode to alleviate the problem. In AC fields, the transmembrane potential generated depends on the field's frequency as described by the Schwan equation^[45]

$$\Delta\psi_{\text{mem}} = \frac{1.5 R_c E}{[1 + (\omega\zeta)^2]^{1/2}} \quad (5)$$

Where $\Delta\psi_{\text{mem}}$ is the transmembrane potential, R_c is the cell's radius, E is the applied electric potential, ω is the frequency of the applied field, and ζ is the membrane capacitance dependent time constant. Hence, while the AC based EP offers lower risk of pH changes due to alternating electrodes, there's a risk of inducing excessive transmembrane potential at low frequencies. However, we observed that a 100 kHz AC field offers favorable membrane dynamics for our biopsy operations so this field parameter was adapted for our biopsy experiments.

Target cells were first prelabeled with calcein AM, while in adherent culture, and cytoplasm extraction was monitored by reduction in green fluorescence intensity. Demonstrations on the NMP's fine spatial precision for targeted single-cell biopsies was then performed on a confluent culture of primary Human Foreskin Fibroblast (HFF) cells (Video S4, Supporting Information). During characterizations, we observed that the cytoplasm extraction rate, indicated by the reduction rate of calcein AM's green fluorescence intensity, is dependent on the applied pk-pk voltage (Figure 4b). This can be attributed to the expected increase in pore size with voltage.

Such characteristics translate to a fine control on the pore sizes in order to either perform reversible EP to extract only a portion of the cell's cytoplasmic content at ≤ 2.5 Vpk-pk (incisional cell biopsy) or completely lyse the cell to collect all of its cytoplasmic content ≥ 3 Vpk-pk (excisional cell biopsy). For incisional biopsies of HFF cells, an average drop of $25\% \pm 10.5\%$ in calcein AM intensity was recorded (Figure 4b,c; and Video S5, Supporting Information). Visual inspection suggested that the integrity of cells that underwent incisional biopsies was retained so we further assessed the possibility of performing multiple biopsies at different time points. In this case, two biopsies were carried out 2 h apart from each other and cell viability, indicative by calcein AM fluorescence, was not significantly affected (Section S9 and Video S6, Supporting Information). This rules out any significant damage to the cell membrane and enforces the suitability of the NMP for performing multiple sampling at different time points and locations to discover cellular response to transient stimuli.

In addition, we demonstrate applicability of our controllable biopsy technique for a range of cell types which include human cancer cell lines and primary mouse embryonic cells, and observed similar trends as with the HFF cells (Figure 4d; and Section S10, Supporting Information). Excisional biopsy of HFF cells were also validated visually with representative images and videos presented in Section S10 and Video S7 (Supporting Information). Upon extraction of all of the cell's cytoplasm via excisional biopsy, we observe that the nucleus remains attached to the substrate, as indicative of the red PI nucleus stain after operation (Section S11, Supporting Information). Subsequent

detachment and extraction of the nucleus was also achieved by physical contact with the electrode and hydrodynamic pull of the aspiration aperture, respectively (Section S11, Supporting Information). This portrays the feasibility of using the NMP to separately analyze cytoplasmic and nuclear contents from the same single-cell for deeper insights into varying gene expressions in the subcellular compartments.^[46] Being able to achieve this while cells are in the adherent state is especially important for analysis of transient biological processes.

The low volume of extracted single-cell cytoplasm (≈ 0.1 pL) necessitated significant dilution for subsequent retrieval with conventional serological steps. As such, in order to validate transcriptome detectability via quantitative polymerase chain reaction (qPCR) amplification, we target the housekeeping RNase-P RNAs with TaqMan probes and primers. Reverse transcription into complementary DNA (cDNA) was performed using a thermal cycler and the resulting cDNA was amplified by qPCR. Samples from the HFF excisional biopsies reached the cycle threshold (Ct) value after an average of 30.8 ± 0.3 cycles, while incisional biopsies samples had an average Ct value of 35.4 ± 0.2 (Figure 4e). These validate the detectability of the sampled RNAs and hence the suitability of the NMP for single-cell transcriptomic and proteomic sampling. As positive control, we quantify the RNase-P RNAs contents from 10 HFF cells preprocessed by chemical lysing and obtained an average Ct value of 28.4 ± 0.1 . Δ Ct between excisional biopsies (1 cell) and the positive control (10 cells) is 2.4, which translates to a measured dilution of 5.27—assuming 100% doubling of DNAs per cycle. This is less than expected but represents a reasonable error range considering difference in protocols and heterogeneity of single-cells. Sampling of EP buffer before the application of the electric field was used as the first negative control (NC1) and no traces of the targeted gene was found after 50 cycles (undetermined Ct). EP buffer was sampled from the culture substrate 5 min after cell biopsies as a second negative control (NC2) and only traces of the RNase-P RNAs were detected with an average Ct of 40.2 ± 0.4 .

2.5. Heat Assisted Whole Cell Dissociation

In Section 2.4, we demonstrated quantification of gene expression using biopsies of cytoplasmic RNA. By isolating cytoplasmic and nuclear transcriptomes, the NMP offers a great capability of quantifying the proportion of mature transcripts within individual cellular compartments, using the same single-cell. However, since the majority of published gene-expression studies have relied on RNAs isolated from whole cells,^[47] an integrated method for retrieving whole single-cells from adherent culture is required for benchmarking. Selective detachment and collection of whole single-cells in adherent culture has been previously demonstrated by the microfluidic probe (dipole configuration).^[25] In this approach, an MFP was used to flush a solution of trypsin over an adherent fibroblast cell for detachment via enzymatic dissociation and collection via hydrodynamic pull. However, since at room temperature, trypsin activity is 1.78 times lower than at optimum temperature of 35.5 °C,^[48] there's room for optimizing this process by simultaneous localized heating of the trypsin reagent.

In order to fully characterize the enzymatic dissociation process of the microfluidic dipole, we first assess the positional bias of the trypsin-HFC in retrieving single-cells at room temperature. With this characterization, we show that the trypsin HFC selectively dissociates HeLa cells with preference given to cells located between the inlet and outlet apertures (Area 1)—coinciding with the maximum flow velocity region (Figure 5a). The average cell dissociation time in Area 1 was about 10 min, which closely correlates with previously reported values.^[25] In order to optimize this process, and hence reduce

the dissociation time, a subtle change in applied voltage was implemented to impose Joule heating, which is described by

$$\Delta T \propto \sigma E^2 \quad (6)$$

Where ΔT is the temperature increase and σ is the electrical conductivity of the solution. For this application, we also increase the AC frequency to 10 MHz to reduce transmembrane potential according to Equation (5). Validation of the NMP's capability to controllably increase the trypsin-HFC's local

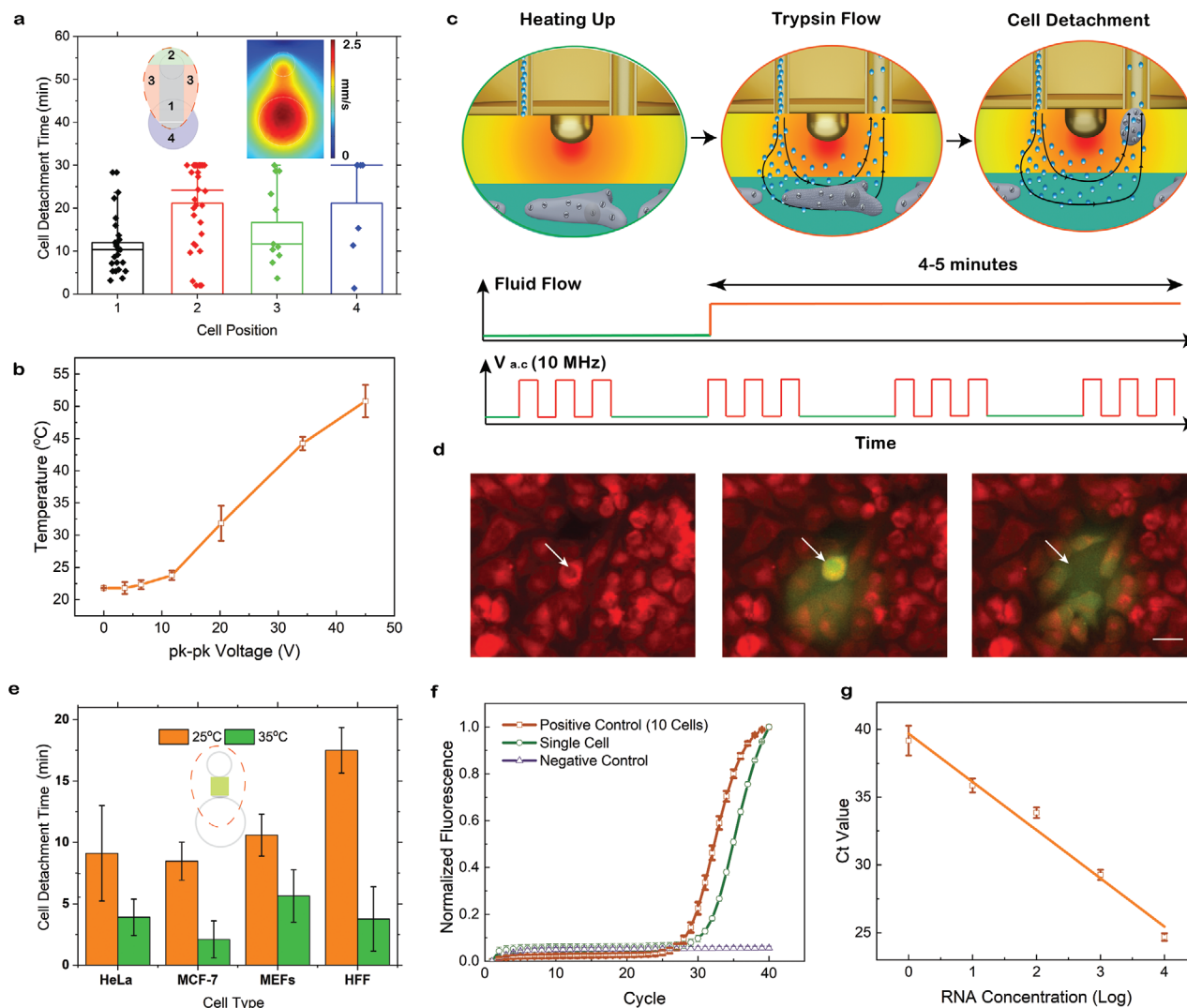


Figure 5. Heat assisted whole cell tweezer. a) Spatiotemporal characterization of trypsin detachment of HeLa cells at room temperature, i.e., no heat assistance. The spatial segmentation (top left inset) and finite element modeling based flow velocity (top right inset) show that detachment time dependency on flow shear stresses. b) NMP's applicability in adjusting localized media temperature. Based on Joule heating, the temperature of the surrounding fluid can be adjusted by varying pk–pk AC voltage at a frequency of 10 MHz. Error bars indicate standard deviation of 4 different separate experiments. c) Step-by-step illustration (top) and time trace (bottom) of the NMP application as a heat assisted single-cell enzymatic dissociation tool. d) Corresponding fluorescence image of HeLa cell culture during the selective NMP's heating up step (left), 2 min after introduction of HFC (middle) and after single-cell tweezing (right). HeLa cells were stained with cell tracker red prior to the experiments to aid visibility. White arrow points to the target cell. Scale bar is 50 μm. e) The single-cell detachment time was significantly reduced at 35 °C based on the optimized trypsin conditions. The target location was also optimized by focusing on the strategic region depicted by the green marking in the inset. f) Mean qPCR amplification curve for RNase P RNAs for tweezed single HeLa cell along with positive control (10 cells preprocessed with chemical lysis), Negative Control 1 (NMP culture media sampling before tweezing). g) Linear range of the qPCR assay based on serial 10X dilution of HeLa cells. The slope is -3.56 and the R^2 value is 0.979 . Error bars in f) and g) indicate standard deviation of four individual measurements.

temperature, based on Joule heating, is presented in Figure 5b. By simultaneously confining single-cells with an HFC of trypsin ($Q_{out}/Q_{in} = 4$) and an AC signal (10 MHz, 22 V_{pk-pk}), we were able to achieve a fluid temperature of 35 °C to optimize dissociation of single-cell targets (Figure 5c,d). The localized heat generation reduced the average dissociation time of HeLa cells by 43.3% and demonstrated similar time improvements in MCF-7, MEFs, and HFF cells (Figure 5e) with no significant impact on the viability of cells retained on the culture substrate (Section S12, Supporting Information).

Upon retrieval, it is important that the cell remains intact to shield the cell contents from trypsin, in order to avoid possible trypsin digestion of internal proteins. We validate that the integrity of the cell membranes is retained by performing reverse transcription and qPCR amplifications of target RNase-P RNAs in the collected single HeLa cell. These resulted in an average Ct value of 31.8 ± 0.08 for RNase P from retrieved single HeLa cells (Figure 5f). As positive control, we performed the same procedure for 10 HeLa cells isolated via serial dilution and obtained an average Ct of 29.2 ± 0.4 . Growth media within the culture dish of the dissociated cell was used as negative control and no target RNA was detected after 50 cycles (undetermined Ct). The validity of these qPCR quantifications was confirmed by obtaining a linear range curve from serial dilution of cDNAs and obtaining a PCR efficiency of 91% and R^2 value of 0.979.^[49] (Figure 5g; and Section S13, Supporting Information). This enforces the ability of the NMP to maintain the membrane integrity of retrieved cells, and hence validates the tools suitability for retrieving the entire transcriptomic, proteomic, and genomic information from a single adherent cell, in a single step.

3. Discussions

The developed NMP technology is a noncontact single-cell manipulation and analysis tool, with multiple spatiotemporal resolved applications. The technology unprecedentedly permits a wide range of multiphysics based single-cell manipulation tasks while retaining overall spatial arrangement in tissue-like cultures. It was invented by leveraging on our previously developed microfluidic probes and multipoles concepts, and single cell resolution was achieved by miniaturization through direct laser 3D printing. The NMP technology is unique in its capability of simultaneously confining reagents and electric fields to a single-cell within tissue cultures, and its integration of electrically enabled subcellular probing features. Further, image recognition models and structural dynamics correlations were implemented for an improved spatial positioning control of the NMP. All of these elements put together a multifunctional setup that is easily adaptable for a broad range of applications.

We demonstrate the application of the NMP for noncontact transfer of extracellular macromolecules through the cell membrane. Targeted delivery of macromolecules in precise patterns was also shown. We performed a comprehensive characterization of EP within adherent cell cultures. Interestingly, the technology aided the discovery of new insights into the dependence of cell morphology on electroporation (EP), which is relevant to the electro-chemotherapy field. Applications of the

NMP for multiplexed single-cell genetic manipulation were also presented. Remarkably, we show the NMP technology as a novel non-contact tool for incisional and excisional biopsies at the single cell level, which are well posed techniques for spatiotemporal resolved single-cell transcriptomic and proteomics sampling. Finally, we validate the applicability of the NMP for retrieving the complete omic information from single-cells either as subcellular compartments or as a whole intact cell.

The concept behind our multiplexed single-cell genetic manipulation is well suited for simultaneous excitation of neurons in vivo. This facilitates an elaborate manipulation of gene expressions within complex neuronal circuits in order to mimic complex brain functions, and hence link our knowledge of single neurons with theories of network functions.^[28] Furthermore, our biopsy techniques present a unique approach for collecting multiple samples at different time points, while retaining the original spatial constraints. This could serve as an invaluable tool for increasing the general knowledge base on organ developmental processes, like cardiac morphogenesis, which still rely on data collected from multiple tissue samples.^[50] Combining the multiplexed single-cell genome engineering and incisional biopsy features of the NMP facilitates sequential spatially resolved programming, and overall omics sampling for multiplexed single-cells. This is indeed a groundbreaking addition to Human Cell Atlas mission^[51]—one of the most ambitious ongoing genomics projects which aims to map all human cells—as our technology introduces a means of retrieving atlas data for samples with engineered genomic diversity. Furthermore, the NMP technology can remarkably integrate other components and concepts, such as stagnation points and zones,^[52] and mixers and biofunctional components^[53] for multiscale cell probing, sampling, isolation, and manipulating.

4. Experimental Section

Cell Culture: HeLa and MCF-7 cells (ATCC, VA) were cultured in sterile Petri Dishes (Thermo Scientific) in Dulbecco's modified Eagle medium supplemented with 10% fetal bovine serum at 37 °C and 5% CO₂ in humidified air. Cells were seeded on ITO-coated glass slides with resistivity of 15–25 Ω sq⁻¹ (Sigma-Aldrich, Saint-Louis) at a density of 500 000 cells mL⁻¹ for 24 h before the experiments. Primary HFF (kind gift from Jeremy Teo lab, NYU Abu Dhabi) and MEFs (kind gift from Mohamed Al Sayegh lab, NYU Abu Dhabi) cells were cultured in the same media and conditions but seeded on the ITO-coated glass slide at density of 150 000 cells mL⁻¹ for 24 h before the experiments. Prior to the transfection and biopsy experiments, the cell culture media was replaced with a low conductivity EP buffer. EP buffer used for the transfection and biopsies experiments was prepared by dissolving 95 g sucrose, 0.1 g dextrose, 3 mL 1 M HEPES solution in 950 mL DI water. The pH was adjusted to 7.4 and conductivity to 140 mS m⁻¹ with 1 M NaOH and DPBS respectively. The osmolarity of the media used for EP was adjusted to 290 mmol kg⁻¹, while that for biopsies was adjusted to 190 mmol kg⁻¹.

Device Fabrication and Assembly: Designs of the NMP, chip-to-holder adapter, and probe holder were created on a commercial CAD software (SolidWorks). The NMP was fabricated in one step using the Nanoscribe Photonics Professional GT system (Nanoscribe GmbH, Eggenstein-Leopoldshafen, Germany) with the commercially available IP-S resin (Nanoscribe GmbH, Eggenstein-Leopoldshafen, Germany). Upon printing, the NMP was soaked in IP-S developer (Nanoscribe GmbH, Eggenstein-Leopoldshafen, Germany) for 24 h, rinsed thoroughly with

ethanol and dried with an air gun. The chip-to-holder adapter was fabricated in one step using a digital light processing (DLP) projector-based stereolithographic 3D printer with a XY resolution of 25 μm (Solus DLP, Junction3D, Santa Clarita, CA). The through holes in the chip-to-holder adapter were fabricated with a 760 μm diameter to accommodate in-house machined metallic tubings (pins) with a 720 μm external diameter. To ensure sterility, the chip-to-holder adapter and pins were subsequently soaked in ethanol for 12 h and rinsed with DI water. The probe holder was also fabricated in one step using the VeroYellow material (Stratasys Rehovot, Santa Clarita, CA) on a PolyJet 3D Printer (Stratasys J750 Stratasys Rehovot, Santa Clarita, CA). The NMP, pins, and chip-to-holder adapter were assembled and affixed together by glue. The assembly was then made conductive by sputtering gold on the entire surface (Cressington Sputter Coater, Ted Peller, CA) until a surface resistivity of $1 \Omega \text{ sq}^{-1}$ was attained. Assembly of these with the probe holder, to form the complete NMP setup, was achieved by the integrated twist lock mechanism.^[32] ITO-coated glass slide ($8\text{--}12 \Omega \text{ sq}^{-1}$, Sigma-Aldrich, Saint-Louis) were used as the counter electrodes and electrical wires were affixed to them using silver conductive epoxy (M.G Chemicals Limited, Ontario, Canada). Electrical contacts to the electrical wires and the NMP were made by clippings. This assembly was mounted on an XYZ micro controller and positioned atop the objective of an inverted microscope.

Finite Element Modeling: The 3D finite element models of the NMP's HFC were developed using a commercial finite element solver (COMSOL Multiphysics v.5.2. COMSOL AB, Stockholm, Sweden). Numerical solutions were acquired by iteratively solving for the coupled Navier–Stokes and convection–diffusion equations. A similar iterative solver was used to compute the continuity equation for the electrical potential. NMPs were modeled as circular surfaces with inlet and outlet apertures and humps on the tip representing the electrode. The injected and immersion fluids were considered as water with a density of 998.2 kg m^{-3} and a dynamic viscosity of 0.001 N-s m^{-2} .

The finite element model used as validation of the correlation between vertical and horizontal displacement of the probe setup was built using a solid mechanics model with linear elastic material properties. The contact between the NMP and the bottom substrate were modeled as a friction contact with a coefficient of friction (CF) = 0.18.

Tip-Substrate Height Adjustment: The NMP assembly was mounted on an XYZ microcontroller (X-LRM Zaber, Vancouver, Canada) and positioned atop of the objective of an Epi-fluorescence inverted ECLIPSE Ti microscope (NIKON, Tokyo, Japan). The ITO-coated glass slide with cells cultured on a portion for 24 h were placed on the microscope stage—in between the objective and the NMP. The Z axis of the XYZ microcontroller is then used to slowly approach a glass slide portion without any cells and monitoring is performed using a combination of a DS-Qi2 camera (NIKON) and the image recognition tool (Code S2, Supporting Information). A horizontal displacement of the NMP is indicative of contact between the probe and the glass slide. Real-time measurement of this displacement for 5 s provides our calibration tool with an input to deduce the upward vertical pull required to zero the tip-substrate gap, based on the correlation deduced and validated in Figure 1f. Upon zeroing, a 20 μm tip-substrate gap is created and the probe is positioned above the target cell using the X and Y axes.

Molecule Transfer Through Cell Membrane: Propidium Iodide (eBioscience, California, United States) and 240 kDa FITC dextran (Sigma-Aldrich, Missouri, USA) were dissolved in the low conductivity EP buffer to final concentrations of 25 ng/mL and 10 mg/mL respectively. Green fluorescein sodium salt (C20H10Na2O5) (Sigma Aldrich, Missouri, USA) was dissolved in the PI-EP solution (final concentration of 1 mg/mL) to aid visibility. The reagent was loaded in syringes, connected to the metallic pins of the NMP assembly via tubings, and controlled by neMESYS high precision syringe pump (CETONI, Korbußen, Germany) to form the HFC. Cell culture media were replaced with EP buffer by gentle rinsing and the whole culture substrate was positioned on the stage of the microscope. Electric potential was created and controlled by a function generator (Keysight

33500B Series, California, US) to produce 1 s DC electric pulses with 50 ms pulse width and 10 Hz frequency during the 3 min cell exposure to the HFC.

The NMP's scanning operation was performed by programming (C#) the XY stage movements in the Zaber scripting environment. The X and Y stages were moved individually for horizontal and vertical lines respectively, and simultaneously for slanted lines (Supplementary Section S5 and Supplementary Codes 2). Spacing between each letter was achieved by rapid movement of the stages ($\sim 29 \text{ mm/s}$), from the end of one letter to the beginning of the other letter (Supplementary Video S2).

Cell Fixing for SEM Imaging: Cells were cultured on a glass slide and at the time of fixing, culture media was replaced with 200 μL of 2% paraformaldehyde (Sigma Aldrich, Missouri, USA). After 15 min of incubation, the paraformaldehyde solution was removed and cells were washed with 10X sterile PBS using a pipette. Cells were then dehydrated by sequential incubation in 50%, 70% and 100% ethanol for 5 min each. The samples were then freeze dried using the Leica EM CPD300 critical point dryer (Leica, Wetzlar, Germany).

Cell Viability: Cell viability after the EP procedure was confirmed by employing a Live/Dead viability/cytotoxicity kit for mammalian cells (Invitrogen, Thermo Scientific, MA, US). For this, cells that underwent EP were incubated in a solution of calcein AM (0.5 μL of 4 mM solution per mL of culture media) and epithidium homodimer-1 (2 μL of 2 mM solution per mL of cell media) for 10 min. After incubation, the Live/Dead viability solution was removed by gently washing with fresh growth media. FITC and TRITC images were obtained with a 20 \times objective and fluorescently labelled Live/Dead cells were manually counted on ImageJ (GNU Library).

Transfection: pCMV-GFP (Addgene plasmid #11153) and mCherry2-C1 (Addgene plasmid # 54563) plasmids were obtained in bacteria as agar stab (Addgene, MA, USA). Individual bacteria colony populations were isolated from the stock by streaking on Luria Broth (LB) agar plates and incubating at 37 $^{\circ}\text{C}$ for 12 – 18 h. LB agar plates were prepared from the powder LB Broth (Miller, Sigma-Aldrich, Saint-Louis, USA) by dissolving 25 g broth powder and 15 g bacteriological agar in 1 L ultrapure water. Ampicillin (100 $\mu\text{g/mL}$) and Kanamycin (50 $\mu\text{g/mL}$) were also dissolved in the LB broth/agar mixture for pCMV-GFP and mCherry2-C1 containing bacteria, respectively. Individual colonies of the bacteria were grown by incubating a swab in 25 mL liquid LB media at 37 $^{\circ}\text{C}$ for 12- 18 h on a shaker. Plasmids were extracted from the bacteria using the QIAprep Spin Miniprep Kit (Qiagen, Hilden Germany), according to the kit's protocol. Quantification of the extracted plasmids were carried out on the NanoDrop (ThermoScientific, MA, US). Purified plasmids were suspended in the EP buffer to a final concentration of 5 ng/mL , loaded into syringes and injected through the inlet aperture of the NMP. Growth media of the cells cultured on the ITO-coated glass slide is replaced with EP buffer and placed on the microscope's stage. A 2 V amplitude DC electric pulse (50 ms pulse) is introduced for 1 s and the target cell is confined by the HFC of fluorescently labelled transfection reagent for 3 min. Note that all HFCs are labelled with green fluorescein sodium salt for visibility and the red colored HFCs are obtained by modification with a red filter on ImageJ. After electroporation, EP buffer is replaced with growth media and the cells are returned back to the incubator for 24 h. Estimation of the transfection efficiency is based on manual counting of the fluorescently labeled cells and the total number of cells covered by the HFC footprint.

Single-Cell Biopsy: To visualize cytoplasmic extraction, cells were pre-labelled with calcein AM (Invitrogen, Thermo Scientific, MA, US). Growth media was replaced with EP buffer and the cells were positioned on the microscope's stage. The NMP was positioned 20 μm above the target cell and a 100 kHz AC electric signal was activated for 1 s to open up the cell membrane, while the HFC buffer was activated for 1 min to extract the content. After extraction, the NMP was pulled up by the Z axis controller and the extracted content was transferred into RNase-free microcentrifuge tubes as a 10 μL solution. As positive control, 10 cells were isolated by serial dilution and lysed in 9 μL of Single-cell Lysis Solution (ThermoScientific, MA, US). Lysing was allowed to continue at

room temperature for 5 min and then stopped using 1 μ L of Single-cell Stop solution (ThermoScientific, MA).

Heat Assisted Single-Cell Enzymatic Dissociation: To enable visibility, cells cultured on the ITO coated glass slide were stained with CellTracker Red CMTPX Dye with a final concentration of 10 μ M. To aid visibility of the HFC, green fluorescein sodium salt (C20H10Na2O5) (Sigma Aldrich, Missouri, USA) was dissolved in Trypsin-EDTA solution (Sigma-Aldrich) with a final concentration of 1 mg/mL. The cells were placed on the microscope's stage and the NMP was positioned 20 μ m above the target cell. Simultaneous activation of the HFC and AC electric signal (10 MHz) effected enzymatic cell dissociation while increasing surrounding media temperature. The AC signal was induced by a function generator (Agilent 33521A, Agilent Scientific Instruments, California, USA) and a high-power amplifier (ZHL-5W-1, Mini Circuits New York, USA) was used to attain voltages greater than 10 V. Upon detachment of the cell, the inlet fluid flow is stopped to allow the suction flow to further dilute trypsin concentration in collected cell suspension. The dissociated cell is then transferred to RNase-free microcentrifuge tubes where they are lysed with Single-cell Lysis Solution (ThermoScientific, MA, US). Voltage dependent temperature measurements were collected by pointing an infrared camera (Flir, Tester UK) at the target area.

Reverse Transcription and Preamplification: Reverse transcription (cDNA synthesis) and pre-amplification of the collected single cell RNAs were performed using a PCR thermal cycler (Labnet MultiGene, Sigma Aldrich, Missouri, USA). The reagents and protocol used are contained in the Ambion Single-cell-to-CT Kit for qRT-PCR (ThermoScientific, MA). Prior to pre-amplification, 1 μ L Single-cell DNase was added to the extracted RNAs. To this, a mixture of Single-cell VILO RT Mix (3 μ L) and Single-cell SuperScript RT (1.5 μ L) were added. Following, the mixture was placed in the thermal cycler for initial priming at 25 $^{\circ}$ C for 10 min, reverse transcription at 42 $^{\circ}$ C for 60 min, and reverse transcriptase inactivation at 85 $^{\circ}$ C for 5 min.

The pre-amplification mixture was prepared by adding 0.2X TaqMan Gene Expression Assay with RNase-P primer (6 μ L) and Single-cell PreAmp Mix (5 μ L) to the reverse transcribed sample. Following, the mixture was held in the thermal cycler for enzymatic activation at 95 $^{\circ}$ C for 10 min, passed through 14 cycles of denaturation at 95 $^{\circ}$ C for 15 s, annealing/extension at 60 $^{\circ}$ C for 4 min, and enzymatic deactivation at 99 $^{\circ}$ C for 10 min.

qPCR: All qPCR amplification experiments were carried out using a StepOnePlus Real-Time PCR System (Applied Biosystems, CA, USA) in MicroAmp Fast Optical 96-Well reaction plates (Applied Biosystems, CA, USA). The TaqMan Probes and Primers were obtained commercially from Applied Biosystems. 4 μ L pre-amplified cDNA was first transferred into the 96-Well reaction plates that contained a mixture of TaqMan Gene Expression Master Mix (10 μ L), TaqMan Gene Expression Assay (1 μ L) and Nuclease-free water (5 μ L). After initial incubation at 50 $^{\circ}$ C for 2 min and enzymatic activation at 95 $^{\circ}$ C for 10 min, 50 PCR cycles were performed (denaturation at 95 $^{\circ}$ C for 5 s, and annealing/extension at 60 $^{\circ}$ C for 1 min). Fluorescence data were recorded at the end of each annealing/extension step.

Supporting Information

Supporting Information is available from the Wiley Online Library or from the author.

Acknowledgements

A.B. acknowledges NYUAD Global Ph.D. Fellowship. This research was funded by NYU Abu Dhabi and the ADEK Excellence Award (AARE19-187) from Abu Dhabi Department of Education and Knowledge, Abu Dhabi, UAE. The authors acknowledge the NYU Abu Dhabi Grants for Publication Program. The authors acknowledge technical support from Dr. James Weston, Dr. Rachid Rezgui, and the rest of the NYUAD core

Technology platforms. They would also like to acknowledge Mei ElGindi and Massar Dieng for support in performing the qPCR experiments.

Conflict of Interest

The authors declare no conflict of interest.

Author Contributions

A.B. and M.A.Q. designed the experiments and developed the setups. M.A.Q. conceptualized the project and supervised the work. A.B. and P.S. carried out the qPCR experiments. A.B. and A.M. performed the EP characterization experiments. A.B. carried out other experiments and numerical simulations. A.B., A.M., and M.A.Q. wrote the manuscript.

Data Availability Statement

The data that support the findings of this study are available from the corresponding author upon reasonable request.

Keywords

biopsy, electroporation, microfluidic probe, single cell, transfection, transcriptomics, tissue culture, tweezing

Received: February 7, 2021

Revised: April 2, 2021

Published online:

- [1] D. Wang, S. Bodovitz, *Trends Biotechnol.* **2010**, *28*, 281.
- [2] K. Klepárník, F. Foret, *Anal. Chim. Acta* **2013**, *800*, 12.
- [3] P. L. Bedard, A. R. Hansen, M. J. Ratain, L. L. Siu, *Nature* **2013**, *501*, 355.
- [4] A. Peng, X. Mao, J. Zhong, S. Fan, Y. Hu, *Proteomics* **2020**, 1900271.
- [5] P. Hu, W. Zhang, H. Xin, G. Deng, *Front. Cell. Dev. Biol.* **2016**, *4*, 116.
- [6] S. M. Prakadan, A. K. Shalek, D. A. Weitz, *Nat. Rev. Genet.* **2017**, *18*, 345.
- [7] X. Xu, J. Wang, L. Wu, J. Guo, Y. Song, T. Tian, W. Wang, Z. Zhu, C. Yang, *Small* **2020**, *16*, 1903905.
- [8] J. D. Buenostro, B. Wu, U. M. Litzenburger, D. Ruff, M. L. Gonzales, M. P. Snyder, H. Y. Chang, W. J. Greenleaf, *Nature* **2015**, *523*, 486.
- [9] I. Tirosh, B. Izar, S. M. Prakadan, M. H. Wadsworth, D. Treacy, J. J. Trombetta, A. Rotem, C. Rodman, C. Lian, G. Murphy, M. Fallahi-Sichani, K. Dutton-Regester, J.-R. Lin, O. Cohen, P. Shah, D. Lu, A. S. Genshaft, T. K. Hughes, C. G. K. Ziegler, S. W. Kazer, A. Gaillard, K. E. Kolb, A.-C. Villani, C. M. Johannessen, A. Y. Andreev, E. M. Van Allen, M. Bertagnolli, P. K. Sorger, R. J. Sullivan, K. T. Flaherty, D. T. Frederick, J. Jané-Valbuena, C. H. Yoon, O. Rozenblatt-Rosen, A. K. Shalek, A. Regev, L. A. Garraway, *Science* **2016**, *352*, 189.
- [10] B. Treutlein, D. G. Brownfield, A. R. Wu, N. F. Neff, G. L. Mantalas, F. H. Espinoza, T. J. Desai, M. A. Krasnow, S. R. Quake, *Nature* **2014**, *509*, 371.
- [11] D. A. Lawson, N. R. Bhakta, K. Kessenbrock, K. D. Prummel, Y. Yu, K. Takai, A. Zhou, H. Eyob, S. Balakrishnan, C.-Y. Wang, P. Yaswen, A. Goga, Z. Werb, *Nature* **2015**, *526*, 131.
- [12] I. L. Brito, S. Yilmaz, K. Huang, L. Xu, S. D. Jupiter, A. P. Jenkins, W. Naisililili, M. Tamminen, C. S. Smillie, J. R. Wortman, B. W. Birren, R. J. Xavier, P. C. Blainey, A. K. Singh, D. Gevers, E. J. Alm, *Nature* **2016**, *535*, 435.

- [13] A. Tanay, A. Regev, *Nature* **2017**, *541*, 331.
- [14] A. Wagner, A. Regev, N. Yosef, *Nat. Biotechnol.* **2016**, *34*, 1145.
- [15] R. Kafri, J. Levy, M. B. Ginzberg, S. Oh, G. Lahav, M. W. Kirschner, *Nature* **2013**, *494*, 480.
- [16] Z. Bar-Joseph, Z. Siegfried, M. Brandeis, B. Brors, Y. Lu, R. Eils, B. D. Dynlacht, I. Simon, *Proc. Natl. Acad. Sci. USA* **2008**, *105*, 955.
- [17] L. Fattore, C. F. Ruggiero, D. Liguoro, R. Mancini, G. Ciliberto, *Cell Death Dis.* **2019**, *10*, 1.
- [18] H. Yu, M. Kortylewski, D. Pardoll, *Nat. Rev. Immunol.* **2007**, *7*, 41.
- [19] R. Yu, Y. Ying, R. Gao, Y. Long, *Angew. Chem., Int. Ed.* **2019**, *58*, 3706.
- [20] Y.-L. Ying, Y.-X. Hu, R. Gao, R.-J. Yu, Z. Gu, L. P. Lee, Y.-T. Long, *J. Am. Chem. Soc.* **2018**, *140*, 5385.
- [21] O. Guillaume-Gentil, E. Potthoff, D. Ossola, C. M. Franz, T. Zambelli, J. A. Vorholt, *Trends Biotechnol.* **2014**, *32*, 381.
- [22] B. P. Nadappuram, P. Cadinu, A. Barik, A. J. Ainscough, M. J. Devine, M. Kang, J. Gonzalez-Garcia, J. T. Kittler, K. R. Willison, R. Vilar, P. Actis, B. Wojciak-Stothard, S.-H. Oh, A. P. Ivanov, J. B. Edel, *Nat. Nanotechnol.* **2019**, *14*, 80.
- [23] O. Guillaume-Gentil, R. V. Grindberg, R. Kooger, L. Dorwling-Carter, V. Martinez, D. Ossola, M. Pilhofer, T. Zambelli, J. A. Vorholt, *Cell* **2016**, *166*, 506.
- [24] C. A. Jordan, E. Neumann, A. E. Sowers, *Electroporation and Electrofusion in Cell Biology*, Springer Science & Business Media, Berlin/Heidelberg, Germany **2013**.
- [25] D. Juncker, H. Schmid, E. Delamarche, *Nat. Mater.* **2005**, *4*, 622.
- [26] N. Anscombe, *Nat. Photonics* **2010**, *4*, 22.
- [27] P. Mukherjee, E. J. Berns, C. A. Patino, E. Hakim Mouly, L. Chang, S. S. P. Nathangari, J. A. Kessler, M. Mrksich, H. D. Espinosa, *Small* **2020**, *16*, 2000584.
- [28] B. Judkewitz, M. Rizzi, K. Kitamura, M. Häusser, *Nat. Protoc.* **2009**, *4*, 862.
- [29] M. Safavieh, M. A. Qasaimeh, A. Vakil, D. Juncker, T. Gervais, *Sci. Rep.* **2015**, *5*, 1.
- [30] P. A. Goyette, É. Boulais, F. Normandeau, G. Laberge, D. Juncker, T. Gervais, *Nat. Commun.* **2019**, *10*, 1781.
- [31] M. A. Qasaimeh, T. Gervais, D. Juncker, *Nat. Commun.* **2011**, *2*, 464.
- [32] A. Brimmo, P. A. Goyette, R. Alnemari, T. Gervais, M. A. Qasaimeh, *Sci. Rep.* **2018**, *8*, 10995.
- [33] A. T. Brimmo, A. Menachery, M. A. Qasaimeh, *Lab Chip* **2019**, *19*, 4052.
- [34] J. F. Henriques, R. Caseiro, P. Martins, J. Batista, *IEEE Trans Pattern Anal. Mach. Intell.* **2015**, *37*, 583.
- [35] J. C. Weaver, *IEEE Trans. Plasma Sci.* **2000**, *28*, 24.
- [36] M. Jordan, F. Wurm, *Methods* **2004**, *33*, 136.
- [37] K. L. Douglas, *Biotechnol. Prog.* **2008**, *24*, 871.
- [38] K. Haas, W.-C. Sin, A. Javaherian, Z. Li, H. T. Cline, *Neuron* **2001**, *29*, 583.
- [39] K. Kinoshita, H. Itoh, S. Ishiwata, K. Hirano, T. Nishizaka, T. Hayakawa, *J. Cell Biol.* **1991**, *115*, 67.
- [40] G. Serša, M. Čemažar, D. Šemrov, D. Miklavčič, *Bioelectrochem. Bioenerg.* **1996**, *39*, 61.
- [41] A. T. Brimmo, M. A. Qasaimeh, *IEEE Nanotechnol. Mag.* **2017**, *11*, 20.
- [42] M. A. Qasaimeh, S. G. Ricoult, D. Juncker, *Lab Chip* **2013**, *13*, 40.
- [43] S. C. Bürgel, C. Escobedo, N. Haandbæk, A. Hierlemann, *Sens. Actuators, B* **2015**, *210*, 82.
- [44] H. H. Wang, F. J. Isaacs, P. A. Carr, Z. Z. Sun, G. Xu, C. R. Forest, G. M. Church, *Nature* **2009**, *460*, 894.
- [45] H. P. Schwan, *Biological Effects and Dosimetry of Nonionizing Radiation*, Springer, Boston, MA **1983**, pp. 213–231.
- [46] M. N. Abdelmoez, K. Iida, Y. Oguchi, H. Nishikii, R. Yokokawa, H. Kotera, S. Uemura, J. G. Santiago, H. Shintaku, *Genome Biol.* **2018**, *19*, 1.
- [47] B. W. Solnestam, H. Stranneheim, J. Hällman, M. Käller, E. Lundberg, J. Lundeberg, P. Akan, *BMC Genomics* **2012**, *13*, 1.
- [48] W. Rick, *Methods of Enzymatic Analysis*, Elsevier, Amsterdam **1974**, pp. 1013–1024.
- [49] D. Svec, A. Tichopad, V. Novosadova, M. W. Pfaffl, M. Kubista, *Biomol. Detect. Quantif.* **2015**, *3*, 9.
- [50] M. Asp, S. Giacomello, L. Larsson, C. Wu, D. Fürth, X. Qian, E. Wärdell, J. Custodio, J. Reimegård, F. Salmén, C. Österholm, P. L. Ståhl, E. Sundström, E. Åkesson, O. Bergmann, M. Bienko, A. Månsson-Broberg, M. Nilsson, C. Sylvén, J. Lundeberg, *Cell* **2019**, *179*, 1647.
- [51] A. Regev, S. A. Teichmann, E. S. Lander, I. Amit, C. Benoist, E. Birney, B. Bodenmiller, P. Campbell, P. Carninci, M. Clatworthy, H. Clevers, B. Deplancke, I. Dunham, J. Eberwine, R. Eils, W. Enard, A. Farmer, L. Fugger, B. Göttgens, N. Hacohen, M. Haniffa, M. Hemberg, S. Kim, P. Klenerman, A. Kriegstein, E. Lein, S. Linnarsson, E. Lundberg, J. Lundeberg, P. Majumder, J. C. Marioni, M. Merad, M. Mhlanga, M. Nawijn, M. Netea, G. Nolan, D. Pe'er, A. Phillipakis, C. P. Ponting, S. Quake, W. Reik, O. Rozenblatt-Rosen, J. Sanes, R. Satija, T. N. Schumacher, A. Shalek, E. Shapiro, P. Sharma, J. W. Shin, O. Stegle, M. Stratton, M. J. T. Stubbington, F. J. Theis, M. Uhlen, A. van Oudenaarden, A. Wagner, F. Watt, J. Weissman, B. Wold, R. Xavier, N. Yosef, Human Cell Atlas Meeting Participants, *Elife* **2017**, *6*, e27041.
- [52] A. T. Brimmo, M. A. Qasaimeh, *RSC Adv.* **2017**, *7*, 5120.
- [53] A. Glia, M. Deliorman, P. Sukumar, F. K. Janahi, B. Samara, A. T. Brimmo, M. A. Qasaimeh, *Adv. Mater. Technol.* **2021**, 2100053.



Supporting Information

for *Small*, DOI: 10.1002/smll.202100801

Noncontact Multiphysics Probe for Spatiotemporal
Resolved Single-Cell Manipulation and Analyses

*Ayoola T. Brimmo, Anoop Menachery, Pavithra
Sukumar, and Mohammad A. Qasaimeh**

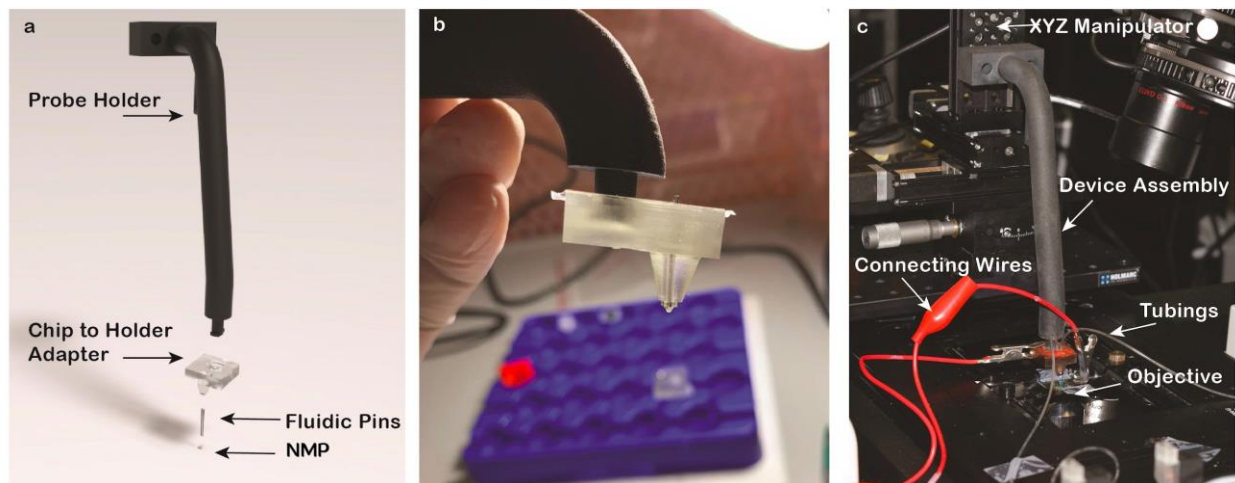
Supplementary Information

Noncontact Multiphysics Probe for Spatiotemporal Resolved Single-Cell Manipulation and Analyses

Ayoola Brimmo, Anoop Menachery, Pavithra Sukumar, Mohammad A. Qasaimeh

Section 1: Device and Experimental Apparatus

The device assembly herein consists of an assembly of a probe holder, chip-to-holder adapter, fluidic pins and the NMP (Fig. S1a). The chip-to-holder adapter, fluidic pins and the NMP are held together by glue and the probe holder is attached to that unit using a twist lock mechanism⁴⁰. A close up view of the device assembly (before gold sputtering) is shown in Fig. S1b. In the experimental setup, the assembly is attached to an XYZ micromanipulator and positioned atop the objective of an inverted microscope (Fig. S1c). Electrical signals from a generator and fluids from syringe pumps are transferred to the device using crocodile clippings and flexible tubings, respectively.



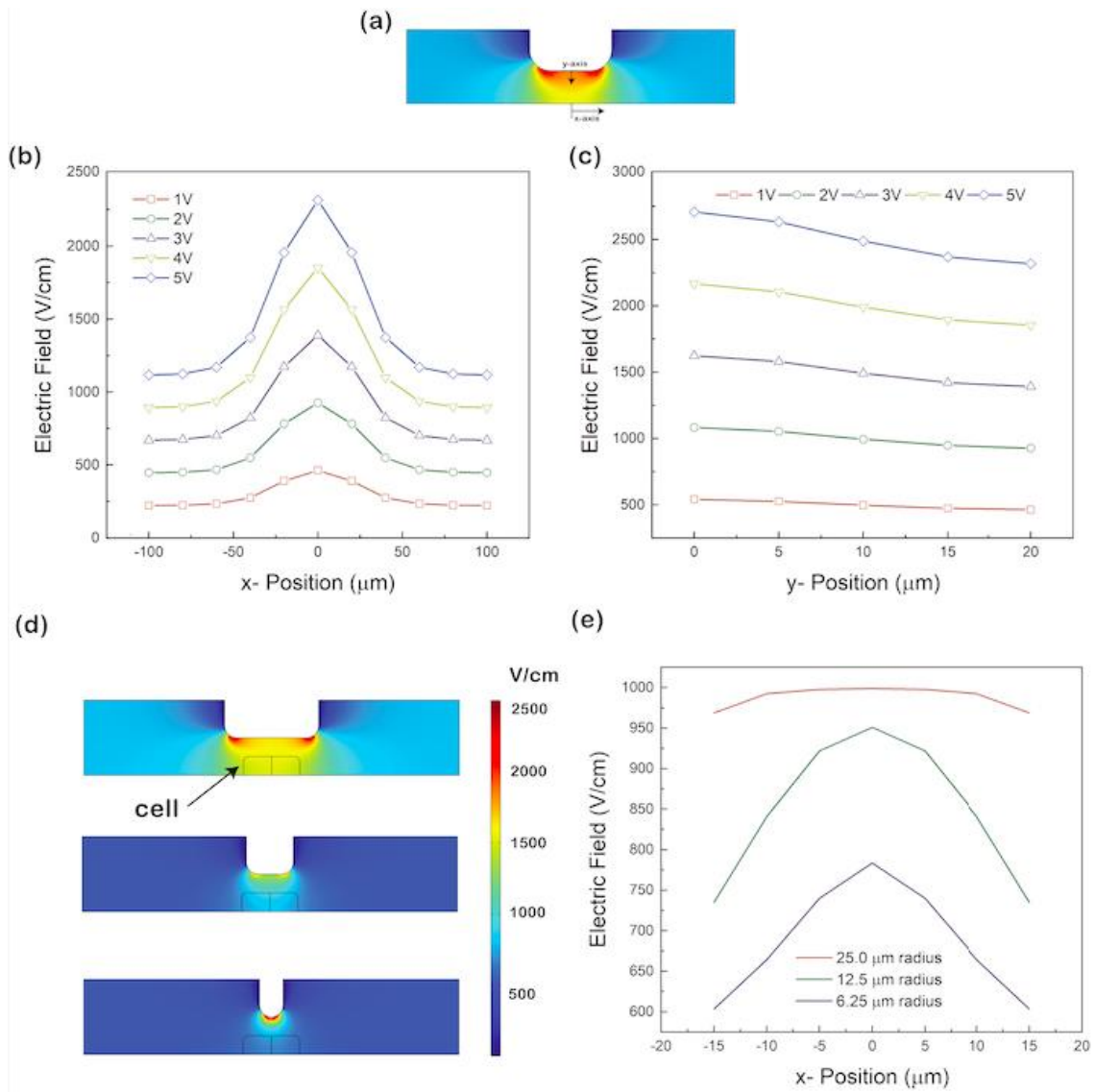
Supplementary Information Fig. S1: **a**, 3D exploded view of the device assembly. **b**, Close up image of the device after assembly. **c**, Image of the experimental setup pointing out the main experimental component.

Section 2: Electrical Field Distribution

Isolation of the electric field was achieved using an integrated pin-plate electrode configuration. In our case, the pin electrode is a 25 μm base radius and height cylindrical “hump” with 10 μm radius fillets on the tip, and the plate electrode is an ITO-coated glass slide. Using finite element modeling, we show that the configuration can isolate high electric fields to the target area directly beneath the electrode (Fig. S2a). The magnitude of the field can be varied by adjusting the applied voltage but regardless of the applied voltage, the high electric field is concentrated within the 50 μm span of the electrode (Fig. S2b). The electric field magnitude also drops across the y -direction as the distance from the electrode

increases. However, for a 20 μm electrode-substrate spacing, the maximum drop is $\sim 15\%$ at the zero x-position (Fig. S2c).

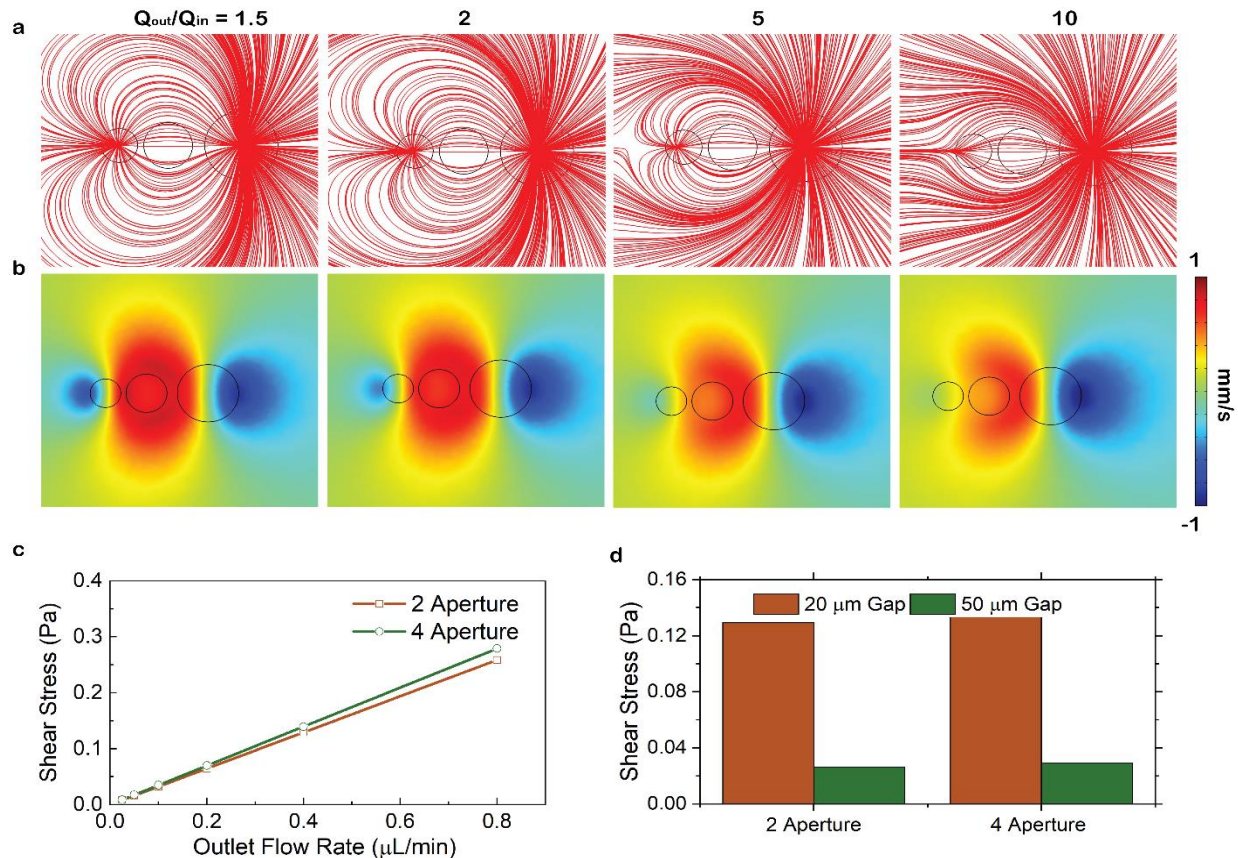
The electrode's diameter also affects the magnitude and distribution of the electric field on the substrate. As the electrode size reduces, concentration of the electric field at the electrode's tip increases and this reduces the magnitude the electric field experienced by target cells (Fig. S2d). Reduced electrode size and hence increased electric field concentration also results in exposure of the cell's cross-sectional area to a non-uniform electric field magnitude (Fig. S2e). Hence, electrode tips less than 25 μm radius are expected to open pores in only the sections of the cells directly beneath the electrode and are hence more beneficial if the intention is to deliver molecules to specific target sections of the cell. In order to open pores across the whole surface of a single cell, and hence increase the chances of molecule delivery to the whole cell, electrode sizes that span across the whole diameter of an average single cell are recommended.



Supplementary Information Fig. S2: **a**, Electrical field contour around the electrode calculated by finite element modeling. **b**, Magnitude of the electric field as a function of applied voltage and the position on the bottom substrate. **c**, Magnitude of the electrical field as a function of the applied voltage and the distance from the electrode at the zero x position. **d**, Electric field contour as a function of electrode size. Electrodes with radius' of 25 μm (top), 12.5 μm (middle) and 6.25 μm (bottom) are positioned 20 μm away from the bottom substrate with a cell represented by a 15 μm radius and 10 μm thick cylinder positioned in between. **e**, Magnitude of the electric field experienced at the top surface of the cell. The 25 μm radius electrode produces a uniform electric field across the cell's surface while those of 12.5 μm and 6.25 μm produces the maximum electric field at the position corresponding to the center of the electrode.

Section 3: Streamlines, Flow Velocity and Shear Stress

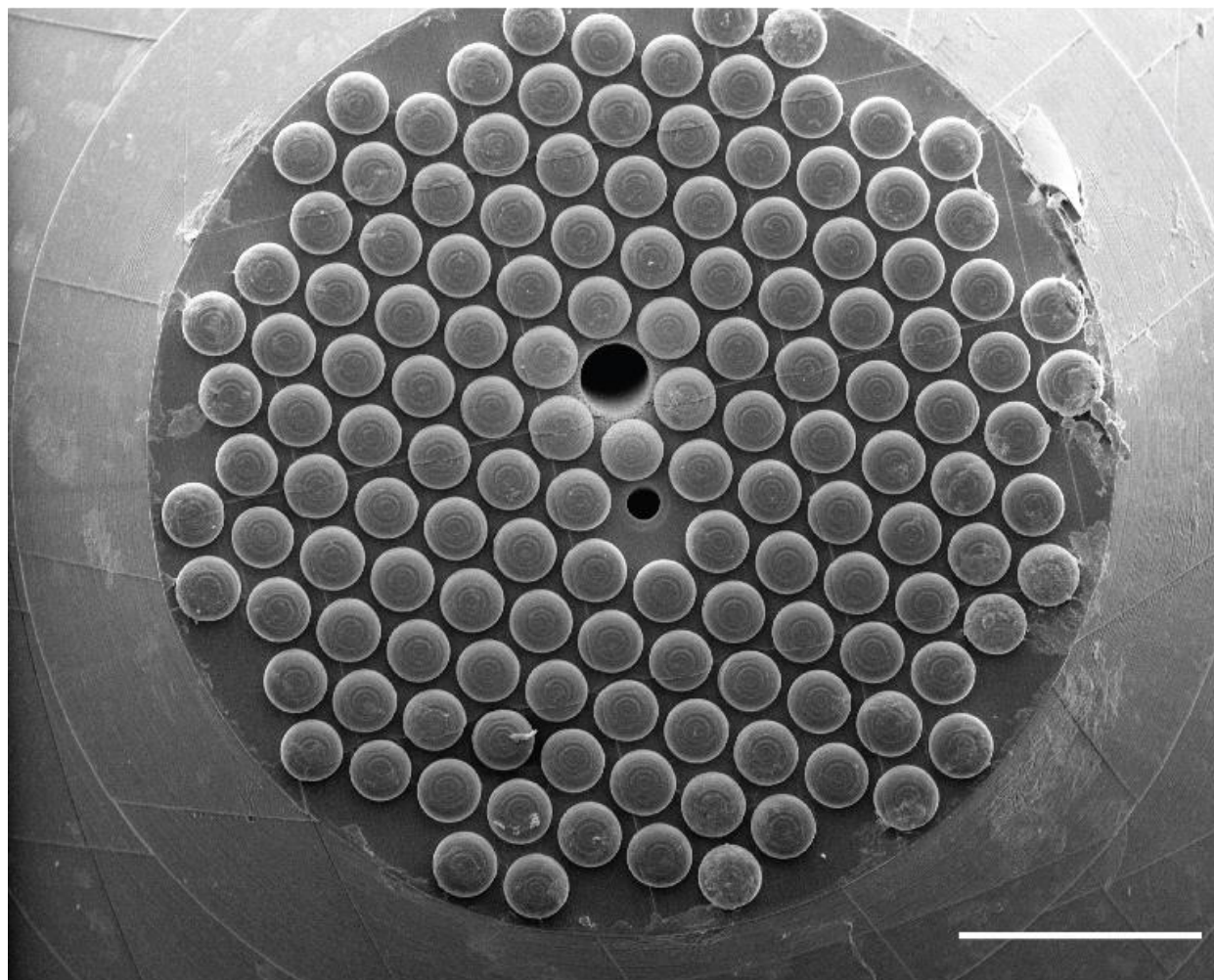
Hydrodynamic flow confinement (HFC) was achieved by simultaneous injection and aspiration through the individual apertures. For a given tip-substrate gap, the ratio of the outlet to inlet aperture flow rates (Q_{out}/Q_{in}) defines the confinement area (Fig. S3a). The fluid velocity at the target area is also affected by Q_{out}/Q_{in} as shown in the velocity contours of Fig. S3b. According to Stokes law, the flow velocity is proportional to the shear stress (τ) imposed on the cell which is given by Equation 4. From the equation, τ is directly proportional to the tangential velocity and inversely proportional to g . Hence for a given Q_{out}/Q_{in} , the shear stress experienced by the target cell is dependent on the flow rate magnitude (Fig. S3c) or the gap g (Fig. S3d).



Supplementary Information Fig. S3: **a**, Flow streamline as a function of Q_{out}/Q_{in} . **b**, Flow velocity contour as a function of Q_{out}/Q_{in} . All figures are results of finite element modelling with a constant Q_{out} of 0.5 $\mu\text{L}/\text{min}$. **c**, Calculated relationship between shear stress and flow rate for $Q_{out}/Q_{in} = 4$. **d**, Calculated relationship between shear stress and electrode-substrate gap.

Section 4: NMP with Broad Span Electrode

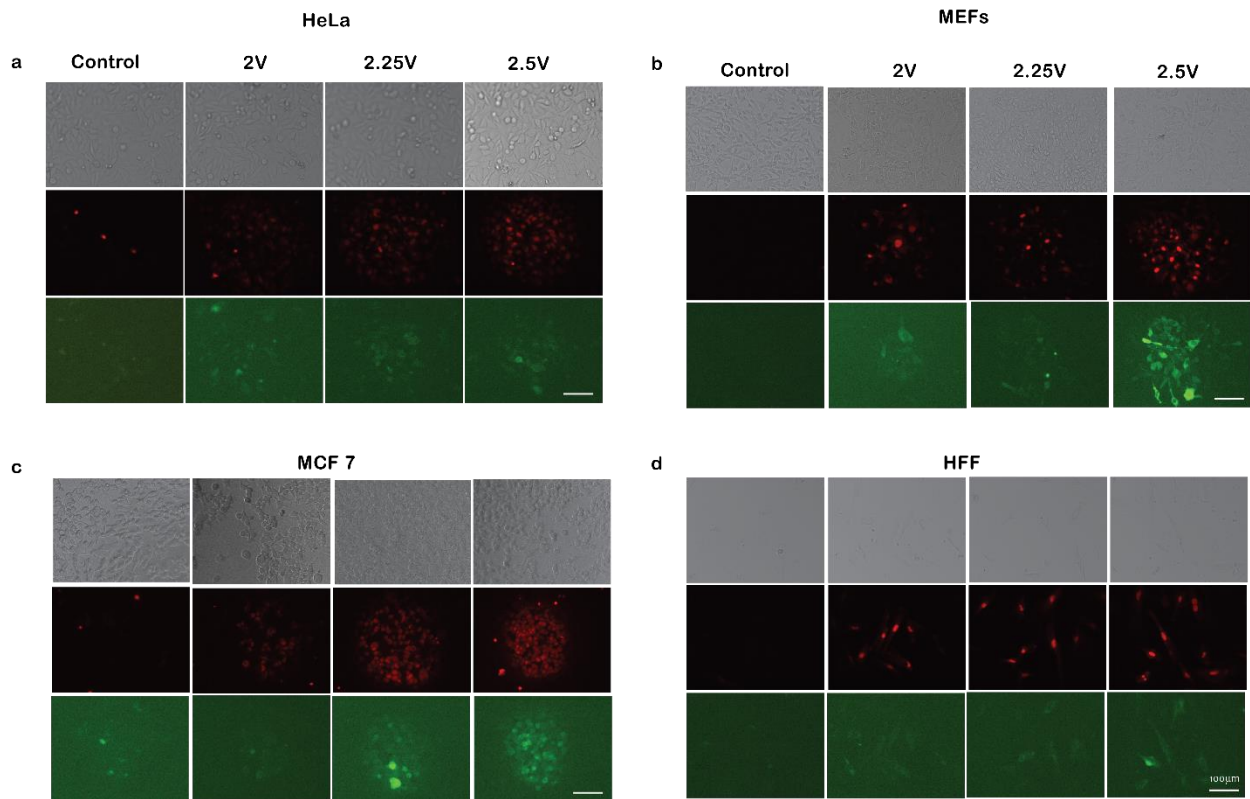
In order to generalize the characterization process, a broad-span electrode version of the NMP was developed by utilizing the entire surface of its tip as an electrode. This was achieved by distributing 138 hump shaped electrodes across the whole tip.



Supplementary Information Fig. S4: Scanning electron microscope images of the NMP with the broad span electrode. Scale bar is 200 μm .

Section 5: Simultaneous PI and FITC Dextran intake

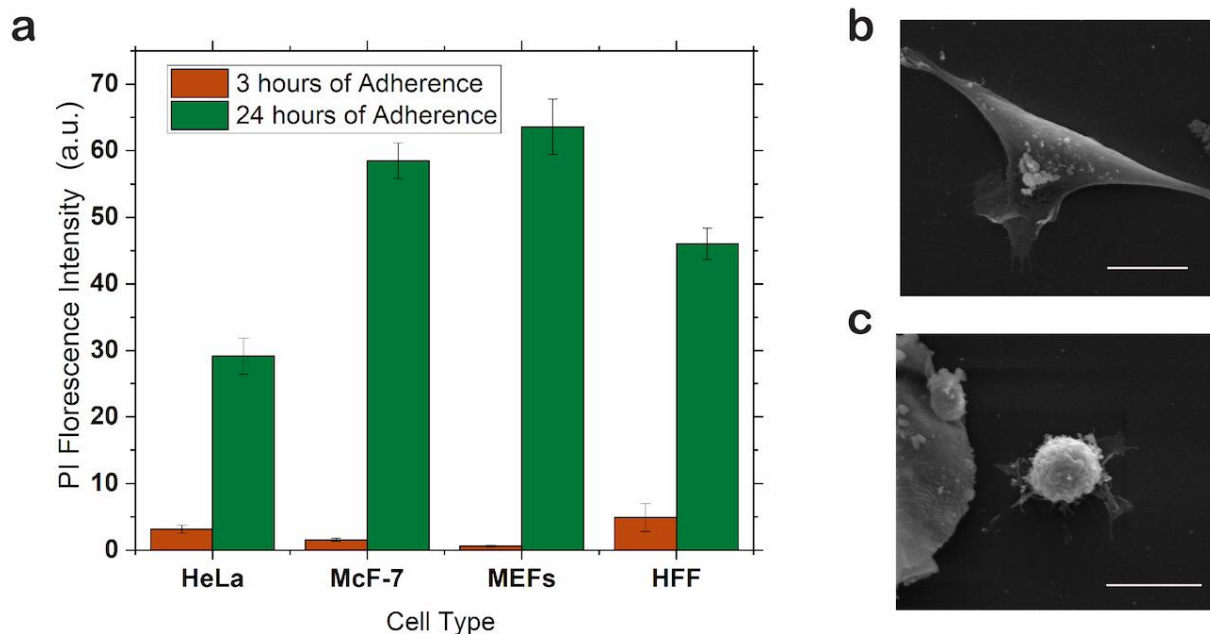
By dissolving PI and FITC Dextran into the EP buffer, we were able to achieve simultaneous transfer of both molecules into target cell clusters. Fig. S5 shows fluorescence mappings of the applied HFC as a function of the peak voltage. The first panel in the image clusters are control experiments where the HFC is applied for a duration of 3 min in the absence of the electric field. Minimal to none PI and FITC dextran fluorescence in these panels demonstrate dependence of the molecule intake on the electric field – with the observed minimal fluorescence attributed to staining of non-viable cells within the culture.



Supplementary Information Fig. S5. Brightfield (top row), PI fluorescence (middle row) and FITC dextran fluorescence for **a**, HeLa. **b**, MEFs. **c**, MCF-7. **d**, HFF cells. $Q_{out}/Q_{in} = 2$, 3 min HFC holding time, and 50 ms pulse width is used for all experiments. Scale bar is 100 μm .

Section 6: Cell Incubation Time and Programmed Scanning Path

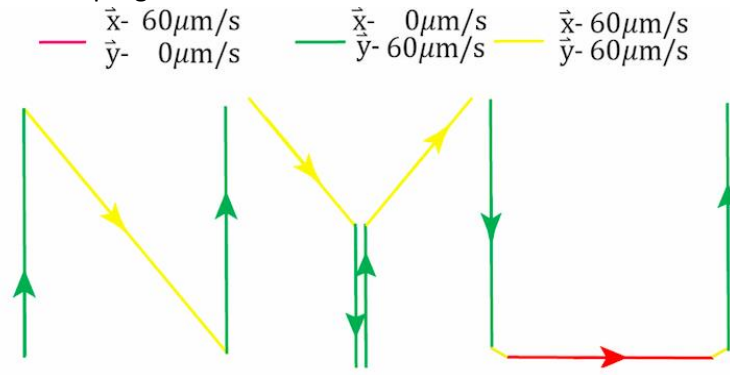
The close proximity between the NMP's electrodes, and the positioning of the target cells relative to the electrodes, permitted the use of low voltage magnitudes to achieve high electric fields. This is the basis behind achieving intake of macromolecules at applied signal amplitudes as low as 2 V. In addition, EP of cells while in adherent culture allowed for an easier membrane penetration in comparison to suspended cells. We validated this by comparing the PI intake at early and advanced stages of adherence. Using the same EP configuration for cells in both stages, increased PI intensity is observed after 24 h of adherence, in comparison to cells allowed to adhere for only 3 h (Fig. S6a). This can be attributed to the high tension state and simplified morphology of adherent cells (Fig. S6b) as opposed to the abundant folds and microvilli presence in the suspended state (Fig. S6c). The reduction of excessive cell membrane area allows for less displacement of electrical stresses leading to higher membrane permeability of stretched lipid bilayers.



Supplementary Information Fig. S6. a, PI intake into cells as a function of time allowed for cell adherence as an indication of a comparison between the EP potential of cells in the adherent and suspended states. Error bars are standard deviation from individual measurements taken on 4 single-cells. **b**, Scanning electron microscope image of a representative MCF-7 cell after 24 h of adherence. **c**, Scanning electron microscope image of a representative MCF-7 cell after 3 h of adherence. The visible presence of folds increases the effective thickness of the cell membrane to reduce increased displacement of electrical stresses. Scale bars in **b** and **c** are 10 μm .

Section 7: Scanning Path and Speed

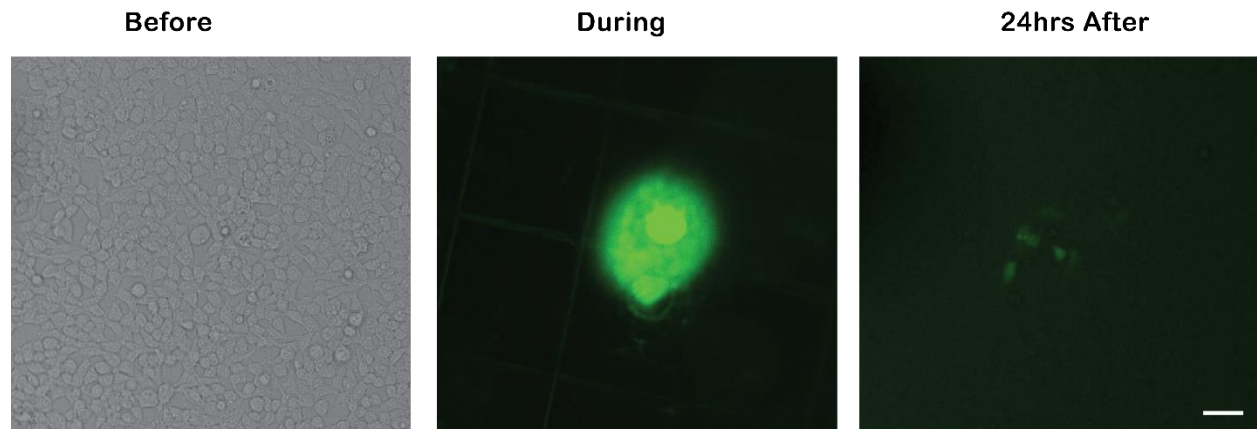
The scanning operation used to create PI intake patterns depend on the individual movement of the micro positioner's X and Y axis to create horizontal or vertical lines respectively, or simultaneous movement of the X and Y axis to create slanted lines. We combined these line types to form the desired "NYU" pattern based on the programmed axis movement scheme shown below.



Supplementary Information Fig. S7. Programmed scanning path and speed for the PI staining with "NYU" pattern.

Section 8: Multiple Cell Transfection

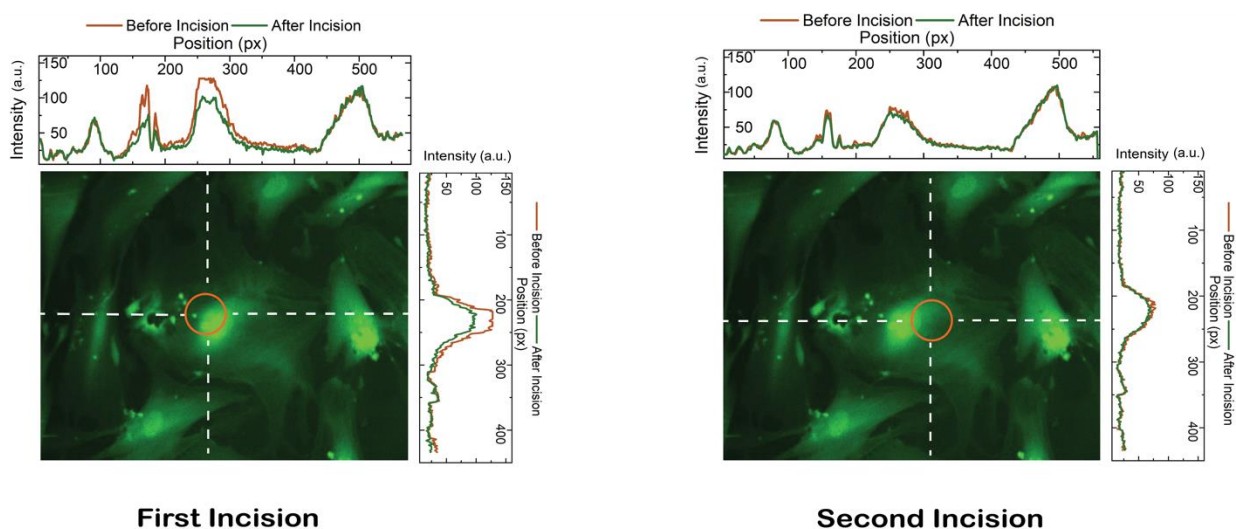
To establish proper genetic functionality of the cells targeted with the broad-span electrode, we demonstrate transfection of MCF-7 cells with a plasmid vector with a green fluorescence protein (PCMV-GFP). The plasmids are delivered by substituting the processing fluid with a mixture of the PCMV-GFP plasmids and the EP buffer. After simultaneous exposure to the HFC ($Q_{out}/Q_{in} = 4$) and the electric field (2 V DC, 10 Hz, 50 ms pulse width, 1 s duration), the cells are returned to the cell culture incubator. FITC fluorescence images after 24 h of incubation shows transfection of about 20% of the target cells. This low transfection efficiency can be attributed to the high degree of variability in the physiological conditions of the cells in adherent culture.



Supplementary Information Fig. S8. Bright field (left), FITC fluorescence during transfection (middle row) and FITC fluorescence 24 h after transfection of a cluster of MCF-7 cells with the PCVM-GFP vector. Scale bar 50 μm .

Section 9: Multiple Time Point Single Cell Biopsy

Incisional biopsies were used to carry out multiple sample extraction at different time points, and different locations, from the same cell. In this example, two biopsies were performed 2 h apart at different membrane locations. Prior to the experiment, cells were stained with calcein AM to monitor permeability and viability in real time. Following each incision, fluorescent signals across sections of the cells are used to estimate the quantity of extracted cytoplasm content and verify localization of the biopsy. After the second biopsy, the cell was found to retain calcein AM fluorescence and ruled out any significant cell damage. The fluorescence intensity drop after the first incision is significantly higher than that of the second incision and we attribute this to higher concentration gradient of calcein AM in the first incision.

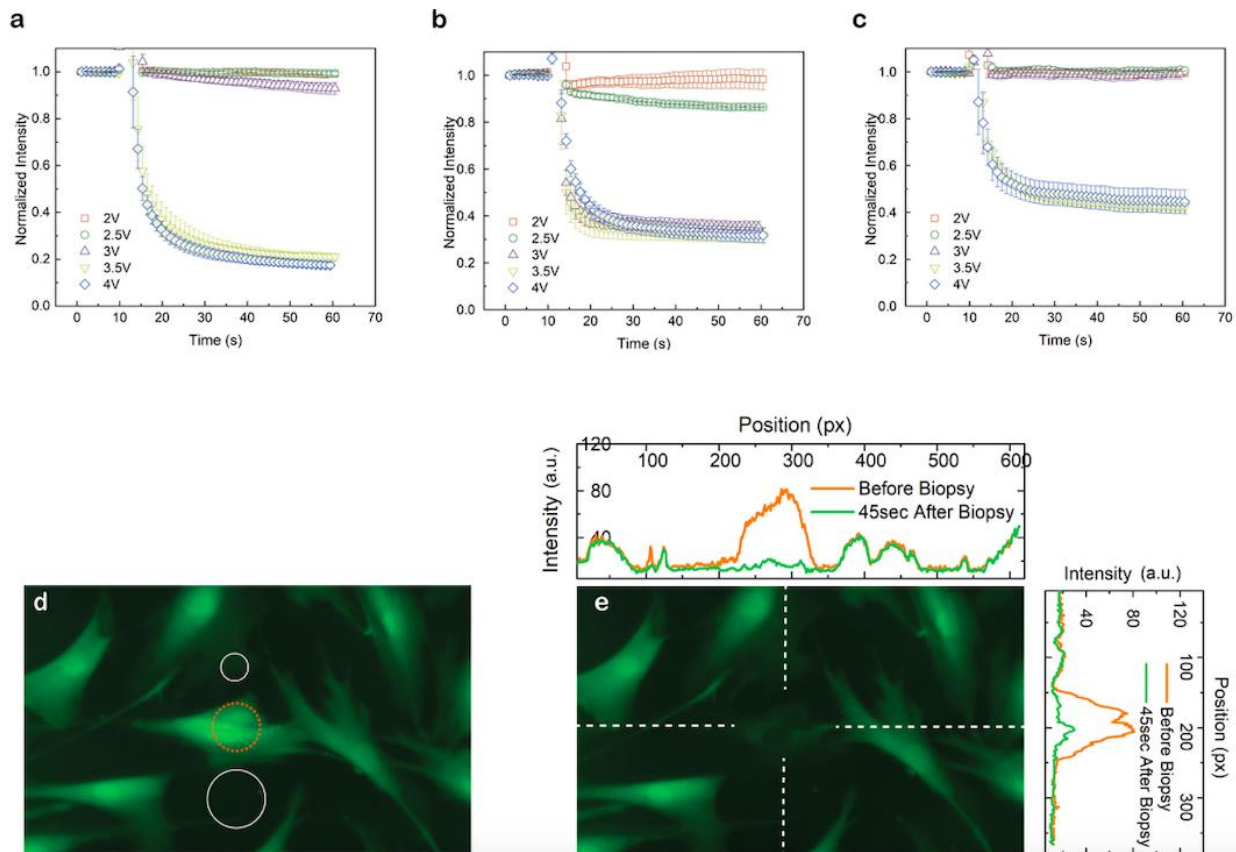


Supplementary Information Fig. S9. Green fluorescence image of HFF cells after multiple time point incisions. Incisional biopsies were made 2 h apart with 2.5 Vpk-pk, 100 kHz AC signals applied for a 1 s duration. White dotted lines represent cross section at which the inset intensity signals are collected and orange circle represents the position of the electrode.

Section 10: Excisional Biopsy and Real-time Cytoplasm Content Monitor

Based on real-time tracking of calcein AM fluorescence intensity, we observed that the transition from incisional to excisional biopsy also falls between 2.5-3 Vpk-pk for HeLa, MCF-7 and MEFs cells (Fig. S10 a-c). However, after incisional biopsies, the average normalized intensity, which is an indication of sampled cytoplasm content, varies with cell types. This can be attributed to the physiological differences between the membranes of different cell types, which is evident from the characterizations of Fig. 2c-g.

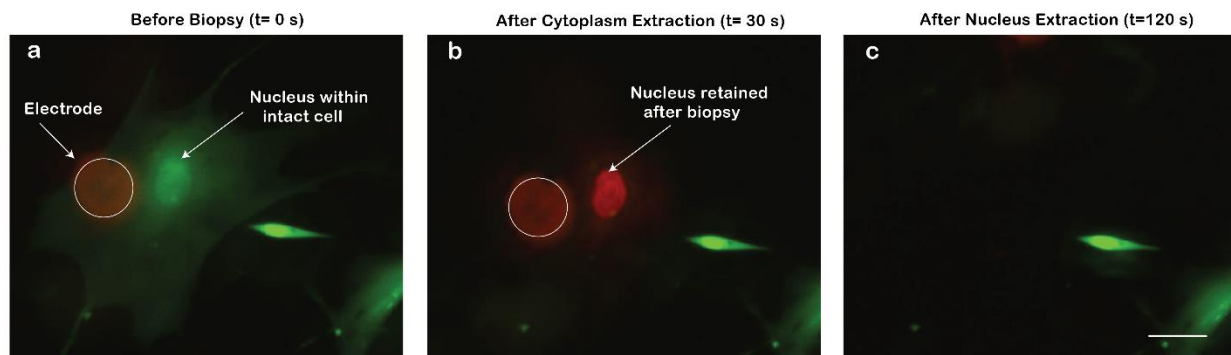
Excisional biopsies were performed on HFF cells and the fluorescence intensity of calcein AM was used to monitor membrane permeability (Fig. S10 d & e). After performing excisional biopsy, calcein AM intensities were observed to drop to levels matching the background intensity of the substrate (inset Fig. S10e). Based on this, we infer that all of the cytoplasmic content has been released and the cell is hence no longer viable.



Supplementary Information Fig. S10. Real-time monitoring of normalized fluorescence intensity during and after the NMP based single cell biopsy of **a**, HeLa. **b**, MCF-7. **c**, MEFs cells. $Q_{out}/Q_{in}=4$, AC frequency of 100 kHz and duration of 1 s. Green fluorescence image of HFF cells before **d**, and after **e**, excisional biopsies using the NMP. Plots on the top and left side of **e** represent quantitative fluorescence intensity across the vertical and horizontal sections highlighted with dotted white lines. The applied electric field in **e** is a 3.5 V AC wave with 100 kHz frequency and 1 s duration.

Section 11: Independent Extraction of Subcellular Compartments

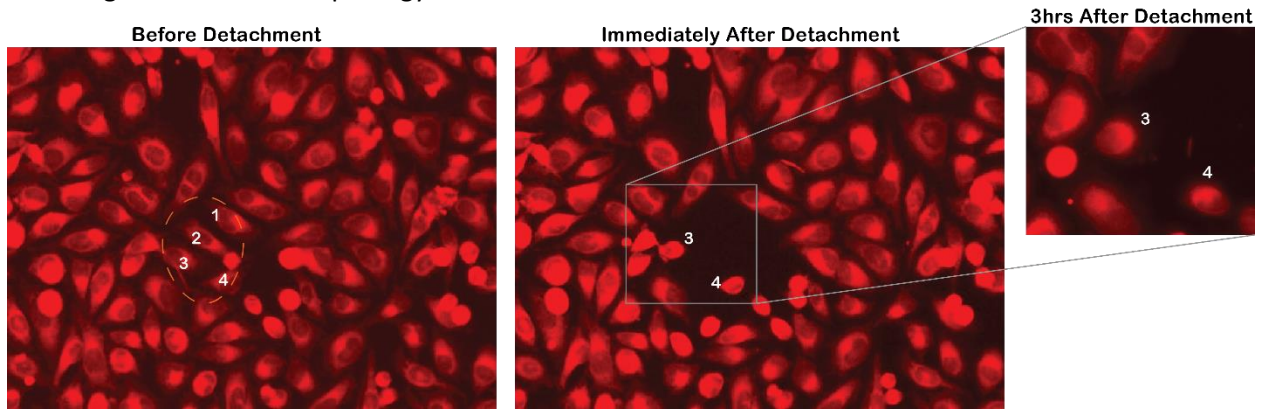
After excisional biopsy, the cell's cytoplasmic content is released to a dedicated aspiration aperture but the nucleus remains attached to the substrate as indicative of the red PI stain. This suggests applicability of the NMP for isolating subcellular compartments of single-cells. The electrode can then be used to physically detach the adherent membrane in order to ease nucleus retrieval from the substrate via hydrodynamic pull of an aspiration aperture. Alternatively, the retained nucleus can be subsequently characterized or sampled using other equipment such as the atomic force microscope for nanomechanical characterization.



Supplementary Information Fig. S11. Separate extraction of single-cell cytoplasm and nucleus. **a**, Target cell before excisional biopsy. Green fluorescence is calcein-AM based representation of intact cells. **b**, After excisional biopsy, the cytoplasmic content of the target cell is released and collected by a dedicated aspiration aperture. PI within the culture media stains the nucleus that remains attached to the substrate. **c**, Lysed cell with retained nucleus retrieved by physical electrode detachment and hydrodynamic pull. Scale bar is 30 μm . The applied AC electric signal is with 3.5 V, 100 kHz, and 1 s duration.

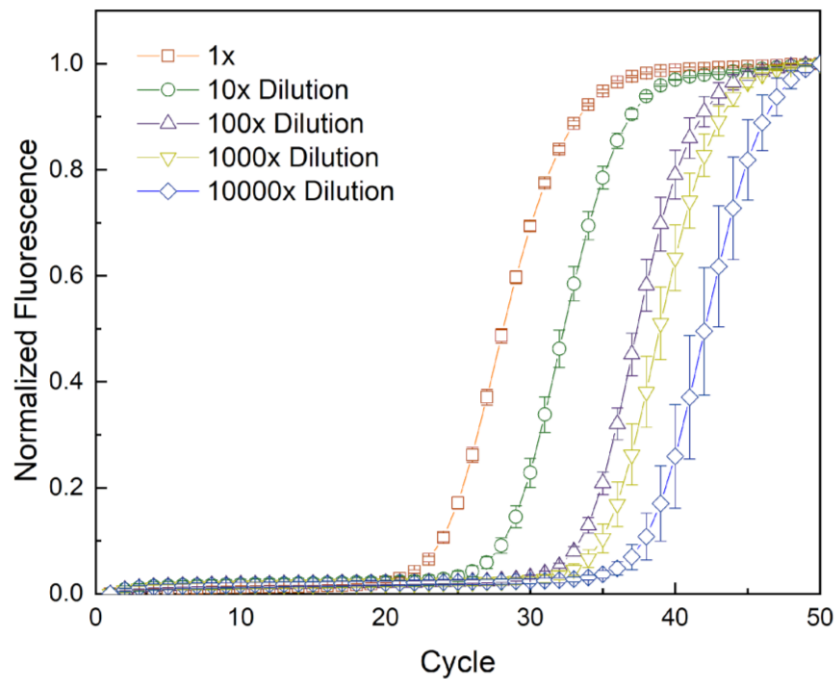
Section 12: Surrounding Cell Regeneration after Single-cell Pick up

In a confluent culture, the HFC created from a 15 μm radius inlet aperture spanned across multiple cells. As such, other cells within the span of the HFC were partially affected by the dissociating effect of trypsin. However, these cells were observed to remain on the substrate and demonstrated recovery of their original adherent morphology after 3 h.



Supplementary Information Fig. S12. Recovery and viability of cells covered by the HFC of Trypsin. Cells 1-4 were confined by the HFC (left) and while the retained cells (3 and 4) show partial dissociation due to interaction with trypsin (middle), they begin to spread out again 3 h after incubation (right).

Section 13: Normalized Ct curves for Linear Range Curve



Supplementary Information Fig. S13. Mean qPCR amplification curve for linear range plot. Error bars indicate standard deviation from 4 different measurements.



Supporting Information

for *Small*, DOI: 10.1002/smll.202100801

Noncontact Multiphysics Probe for Spatiotemporal
Resolved Single-Cell Manipulation and Analyses

*Ayoola T. Brimmo, Anoop Menachery, Pavithra
Sukumar, and Mohammad A. Qasaimeh**

Supplementary Video 1: Detecting zero tip-substrate gap using image recognition (Fig. 1f)

Video showing use of the Kernelized Correlation Filters (KCF) image recognition module to track the onset of the NMP's horizontal displacement (HD) which signifies zero tip-substrate gap. The width of the tracked aperture is entered in micrometers in order to convert the position coordinates to micrometers. "X Position" and "Y Position" signifies the x- and y- coordinates of the bounding box's centroid. Increase in "X Position" indicates HD and hence the onset of zero tip-substrate gap. The python codes used to automate this process is provided in the Supplementary Codes section.

Supplementary Video 2: NMP as scanning probe for spatially resolved electropermealization (Fig. 2f).

Operating the NMP as a scanning probe to introduce a red impermeable dye (propidium iodide) into MCF-7 cells with a pattern that spelt "NYU". Electropermealization (EP) was performed by simultaneous localized exposure of target cells to an HFC of PI dissolved in EP buffer and 2V-10Hz rectangular DC pulses with 50 ms pulse width. Scanning velocities for each type of line is presented in Supplementary Section 7 and the code used to automate the stage's movement is provided in the Supplementary Codes section.

Supplementary Video 3: EP based transfer of macromolecule into single HeLa cell.

Targeting single HeLa cell with simultaneous localized HFC and electric field to introduce propidium iodide (PI) into the cell. The electric field (2V DC rectangular pulse with 10Hz frequency and 1 s duration) is activated between 00:00:03:00 and 00:00:04:00, and PI introduction is indicated by the subsequent increasingly intense red fluorescence stain.

Supplementary Video 4: Single-cell biopsy from a confluent culture of HFF cells.

NMP biopsy based extraction of the cytoplasm of a single HFF cell within an adherent culture. All cells are pre-labelled with calcein AM and cytoplasm extraction is inspected by reduction in fluorescence intensity. The red arrow points to the target cell. At 00:00:03:00, the electrode is lowered to a position 20 μm above the target cell. Between 00:00:05:00 and 00:00:06:00, the electric field is activated and the green fluorescence intensity of the target cell drops. At 00:00:20:00, the electrode is lifted to get rid of the background fluorescence introduced by the electrode. The applied electric field is generated by a 3V AC wave with 100 kHz frequency and 1 s duration.

Supplementary Video 5: Single-cell incisional biopsy (Fig. 4c).

Video demonstrating targeted incisional biopsy (partial cytoplasmic content retrieval) of a single HFF cell. At the beginning of the video, the NMP is positioned 2 mm above the cell to avoid interference of the background fluorescence. The red arrow points to the target cell. At 00:00:05:00, the device is lowered till a 20 μm electrode-substrate gap is attained. The electric field is activated between 00:00:05:00 and 00:00:06:00 and the NMP is lifted back up immediately after. Lowering and lifting of the NMP are necessary to avoid interference of background intensities before and after the biopsy procedure. Fig. 4b quantifies fluorescence intensity during the process and inset Fig. 4c shows the spatially resolved intensities before and after incisional biopsies. The applied electric field is generated by a 2.5V AC wave with 100 kHz frequency and 1 s duration.

Supplementary Video 6: Multiple time point incisional biopsy (Fig. S9).

A single HFF cell was targeted with a 2.5V AC wave with 100 kHz frequency and 1 s duration at two different time points 2 h apart. Incisional biopsy samples were collected at both times and the cell remained viable after the operation. For the first incision, the NMP is lowered at 00:00:04:00 and the electric field is activated between 00:00:05:00 and 00:00:06:00. Lowering of the NMP for the second incision is at 00:00:19:00 and activation of the electric field is at 00:00:21:00. Quantification of the drop in fluorescent intensity for both incisions are presented in Supplementary Section 9. The applied electric field for both incisions are generated by a 2.5V AC wave with 100 kHz frequency and 1 s duration.

Supplementary Video 7: Single-cell excisional biopsy (Fig. S10e).

Video showing targeted excisional biopsy (full cytoplasmic content retrieval) of a single HFF cell. The red arrow points at the target cell. At 00:00:05:00, the device is lowered till a 20 μm electrode-substrate gap is attained. Between 00:00:05:00 and 00:00:06:00, the electric field is activated and the green fluorescence intensity of the target cell drops. At 00:00:28:00, the electrode is lifted to remove the background fluorescence introduced by the electrode. The applied electric field is generated by a 3.5 V AC wave with 100 kHz frequency and 1 s duration.